AD-A070 480 MARYLAND UNIV COLLEGE PARK DEPT OF PHYSICS AND ASTRONOMY F/G 20/9
INFLUENCE OF FINITE ION LARMOR RADIUS EFFECTS ON THE ION RESONA--ETC(U)
1977 R C DAVIDSON, H UHM N00014-75-C-0309
UNCLASSIFIED PUB-77-246 NL

| OF |
AD
A070480

END
DATE FILMED
7-79
DDC

PREPRINT #705P004

INFLUENCE OF FINITE ION LARMOR RADIUS EFFECTS ON THE ION RESONANCE INSTABILITY IN A NONNEUTRAL PLASMA COLUMN

Ronald C. Davidson
Division of Magnetic Fusion Energy
Energy Research and Development Administration
Washington, D. C. 20545

and

Faculty of Science
Hiroshima University, Hiroshima, Japan

Hwan-sup Uhm
Department of Physics and Astronomy
University of Maryland, College Park, Md. 20742

Physics Publication Number 77-246

Work on this report was supported by ONR Contract N00014-75-C-0309 and/or N00014-67-A-0239 monitored by NRL 6702. 02.

1977

UNIVERSITY OF MARYLAND
DEPARTMENT OF PHYSICS AND ASTRONOMY
COLLEGE PARK, MARYLAND

DDC PROCESSING DATA

PHOTOGRAPH

THIS SHEET

RETURN TO DDA-2 FOR FILE

II
LEVEL

1
INVENTORY

AD A070480
DDC ACCESSION NUMBER

Preprint 705P004, Physics Pub. 77-246
DOCUMENT IDENTIFICATION

DISTRIBUTION STATEMENT A
Approved for public release;
Distribution Unlimited

DISTRIBUTION STATEMENT

Accession For
NTIS GRA&I
DDC TAB
Unannounced
Justification
By
Distribution/
Availability Codes
Dist. | Avail and/or special
A

DISTRIBUTION STAMP

DDC
RECEIVED
JUN 28 1979
D

DATE ACCESSIONED

79 06 27 314

DATE RECEIVED IN DDC

PHOTOGRAPH THIS SHEET

RETURN TO DDA-2

INFLUENCE OF FINITE ION LARMOR RADIUS EFFECTS ON THE ION RESONANCE INSTABILITY IN A NONNEUTRAL PLASMA COLUMN

Ronald C. Davidson*
Division of Magnetic Fusion Energy
Energy Research and Development Administration
Washington, D. C. 20545

and

Faculty of Science
Hiroshima University, Hiroshima, Japan

Hwan-sup Uhm
Department of Physics and Astronomy
University of Maryland, College Park, Md. 20742 USA

This paper investigates the influence of finite ion Larmor radius effects on the ion resonance instability in a nonneutral plasma column aligned parallel to a uniform axial magnetic field $B_0\hat{e}_z$. The analysis is carried out within the framework of a hybrid Vlasov-fluid model in which the ions are described by the Vlasov equation and the electrons are described as a macroscopic, cold fluid. Electrostatic stability properties are calculated for the case in which the equilibrium electron and ion density profiles are rectangular and the ion distribution function is specified by $f_i^0=\text{const.}\times\delta(H_\perp-\omega_i P_\theta-\hat{T}_i)G(v_z)$. The resulting eigenvalue equation for the perturbed electrostatic potential $\hat{\phi}_\ell(r)$ is solved exactly to give a closed algebraic dispersion relation for the complex eigenfrequency ω. This dispersion relation is solved numerically, and it is shown that the growth rate of the ion resonance instability exhibits a sensitive dependence on plasma parameters. For example, finite ion Larmor radius effects can have a strong stabilizing influence for azimuthal mode numbers $\ell\geq 2$, particularly when the equilibrium self electric field is sufficiently weak. For the fundamental mode ($\ell=1$), however, stability properties are identical to those calculated from a macroscopic two-fluid model, and the growth rate is unaffected by the value of ion Larmor radius.

*On leave of absence from the University of Maryland, College Park, Md.

1. INTRODUCTION

One of the most basic instabilities that characterizes a nonneutral plasma[1] with both ion and electron components is the ion resonance instability.[2-5] In cylindrical geometry (Fig. 1), the ion resonance instability can be described as a two-rotating-stream instability[2] in which the relative rotation between electrons and ions is produced by the equilibrium self-electric field $E_r^0(r)\hat{e}_r$. Previous analyses of this instability have been based on macroscopic cold-fluid models[2-4] in which the ion and electron motion is assumed to be laminar. Although this is a reasonable approximation when

$$\hat{r}_{Li} \ll R_p ,$$

we expect significant modifications to the stability behavior when $\hat{r}_{Li} \tilde{>} R_p$. (Here $\hat{r}_{Li}$ is the characteristic thermal ion Larmor radius, and R_p is the radius of the plasma column.) In this paper, we investigate the influence of finite ion Larmor radius effects on the ion resonance instability in a nonneutral plasma column with rectangular electron and ion density profiles (Fig. 2). The analysis is carried out within the framework of a hybrid Vlasov-fluid model. The electrons are described as a macroscopic, cold ($T_e \to 0$) fluid immersed in a uniform axial magnetic field $B_0\hat{e}_z$. On the other hand, to allow for the possibility of large ion orbits with thermal Larmor radius comparable to the radius of the plasma column, we adopt a fully kinetic model for the ions in which the ions are described by the Vlasov equation. Such hybrid models have also proven quite tractable in theta-pinch[6,7] and ion-layer[8] applications.

The stability studies presented here assume electrostatic perturbations with infinitely long axial wavelengths ($\partial/\partial z=0$). Moreover, the analysis is carried out for arbitrary values of the dimensionless parameter

$$\alpha \equiv \frac{\hat{r}_{Li}}{R_p} .$$

For a nonneutral plasma column with uniform density, it is also useful to introduce the dimensionless parameter

$$\delta \equiv \frac{2\hat{\omega}_{pe}^2}{\omega_{ce}^2} (1-f) ,$$

which is a measure of the characteristic relative strengths of the equilibrium self-electric force and the magnetic force on an electron fluid element. Here $\hat{\omega}_{pe}$ is the electron plasma frequency, ω_{ce} is the electron cyclotron frequency, and $f=n_i^0/n_e^0$ is the fractional charge neutralization provided by the positive ions. In the present analysis, the parameter δ and the fractional charge neutralization are allowed to span the range of values

$$0<\delta\leq 1 ,$$

and

$$0\leq f\leq 1 ,$$

where $\delta=1$ corresponds to the maximum allowed charge density for radial confinement of the equilibrium configuration.

The outline of this paper is the following. In Sec. 2, we describe the hybrid Vlasov-fluid model (Sec. 2.A) and summarize the equilibrium formalism (Sec. 2.B) for general electron density profile $n_e^0(r)$ and equilibrium ion distribution function of the form[9]

$$f_i^0 = f_i^0$$

Here, v_z is the axial velocity, $H_\perp$ is the perpendicular energy [Eq. (9)], P_θ is the canonical angular momentum [Eq. (10)], and ω_i= const. In Sec. 2.C, equilibrium properties are calculated for the case where the electron and ion density profiles are rectangular (Fig. 2) and the ion distribution function is specified by [Eq. (18)]

$$f_i^0(\mathcal{H},\mathcal{P}) = \frac{f n_0 m_i}{2\pi}\,\delta(H_\perp-\omega_i P_\theta-\hat{T}_i)G(v_z)\ ,$$

where f, n_0 and $\hat{T}_i$ are constants. Electrostatic stability properties are discussed in Secs. 3 and 4. In Sec. 3.A, the general eigenvalue equation [Eq. (49)] is formulated for arbitrary $n_e^0(r)$ and $f_i^0(H_\perp-\omega_i P_\theta,\ v_z)$. In circumstances where the perturbed ion density corresponds to a surface-charge perturbation (at $r=R_p$), the eigenvalue equation (49) is then solved in Secs. 3.B and 3.C for the case where f_i^0 is specified by Eq. (18) and the electron and ion density profiles are rectangular. A striking feature of this analysis is the fact that the required orbit integral $\hat{I}$ [Eq. (50)] can be evaluated in closed form [Eqs. (59) and (62)] for general values of the parameters $\hat{r}_{Li}/R_p$ and $(2\hat{\omega}_{pe}^2/\omega_{ce}^2)(1-f)$. Moreover, the resulting eigenvalue equation (61) for the perturbed electrostatic potential $\hat{\phi}_\ell(r)$ can be solved exactly to give a closed algebraic dispersion relation [Eq. (66)] for the complex eigenfrequency ω. As expected, in the limit where $\alpha=\hat{r}_{Li}/R_p\to 0$, Eq. (66) reduces to the familiar cold-fluid dispersion relation [Eq. (70)] previously discussed in the literature.[2,3]

The general dispersion relation (66) is an algebraic equation of order $\ell+3$, where ℓ is the azimuthal mode number. In Sec. 4, a detailed numerical analysis of Eq. (66) is presented and stability properties are investigated for a broad range of plasma parameters.

It is found that the growth rate of the ion resonance instability exhibits a very sensitive dependence on $\hat{r}_{Li}/R_p$, $\hat{\omega}_{pe}^2/\omega_{ce}^2$ and f. For example, finite ion Larmor radius effects can have a strong stabilizing influence for mode numbers $\ell \geq 2$ (see, for example, Figs. 10 and 14), particularly when the equilibrium self-electric field is weak ($\hat{\omega}_{pe}^2/\omega_{ce}^2 \ll 1$ or f close to unity). For the fundamental mode ($\ell=1$), however, stability properties are identical to those calculated from a macroscopic two-fluid model, and the growth rate is unaffected by the value of $\hat{r}_{Li}/R_p$.

As a final note, we emphasize that the present stability studies are based on a fully nonlocal analysis of the linearized ion Vlasov equation. The fact that the dispersion relation can be obtained in closed form is a somewhat fortuitous manifestation of the sharp-boundary feature of the equilibrium configuration (Fig. 2) and the choice of equilibrium ion distribution function in Eq. (18).

2. THEORETICAL MODEL AND EQUILIBRIUM PROPERTIES

2.A Theoretical Model

In the present analysis, the electrons are treated as a cold ($T_e \to 0$) fluid immersed in a uniform axial magnetic field $B_0 \hat{e}_z$. Within the context of the electrostatic approximation ($\underset{\sim}{B} \simeq B_0 \hat{e}_z$ and $\nabla \times \underset{\sim}{E} \simeq 0$), the equation of motion and the continuity equation for the electron fluid can be expressed as

$$\left(\frac{\partial}{\partial t} + \underset{\sim}{V}_e \cdot \nabla\right)\underset{\sim}{V}_e = -\frac{e}{m_e}\left(-\nabla\phi + \frac{\underset{\sim}{V}_e \times B_0 \hat{e}_z}{c}\right) , \tag{1}$$

$$\frac{\partial}{\partial t} n_e + \nabla \cdot (n_e \underset{\sim}{V}_e) = 0 , \tag{2}$$

where $\underset{\sim}{E}(\underset{\sim}{x},t) = -\nabla\phi(\underset{\sim}{x},t)$ is the electric field, $n_e(\underset{\sim}{x},t)$ is the electron density, $\underset{\sim}{V}_e(\underset{\sim}{x},t)$ is the mean electron velocity, and $-e$ and m_e are the electron charge and mass, respectively. In Eq. (1), the spatial variation in B_0 is neglected (low-beta approximation).

To allow for the possibility of large ion orbits with thermal Larmor radius comparable with the radius of the plasma column, we adopt a fully kinetic model in which the ion distribution function $f_i(\underset{\sim}{x},\underset{\sim}{v},t)$ evolves according to the Vlasov equation

$$\left\{\frac{\partial}{\partial t} + \underset{\sim}{v} \cdot \frac{\partial}{\partial \underset{\sim}{x}} + \frac{e}{m_i}\left(-\nabla\phi + \frac{\underset{\sim}{v} \times B_0 \hat{e}_z}{c}\right) \cdot \frac{\partial}{\partial \underset{\sim}{v}}\right\} f_i(\underset{\sim}{x},\underset{\sim}{v},t) = 0 , \tag{3}$$

where $+e$ and m_i are the ion charge and mass, respectively. In Eqs. (1)-(3), the electrostatic potential $\phi(\underset{\sim}{x},t)$ is determined self-consistently from Poisson's equation

$$\nabla^2\phi = -4\pi e\left(\int d^3v f_i - n_e\right) . \tag{4}$$

Equations (1) - (4) constitute a closed description of the equilibrium and electrostatic stability properties of the nonneutral plasma column, and form the theoretical basis for the subsequent analysis.

2.B General Equilibrium Properties

An equilibrium analysis of Eqs. (1)-(4) for general steady-state ($\partial/\partial t=0$) profiles proceeds in the following manner. As illustrated in Fig. 1, we introduce cylindrical polar coordinates (r,θ,z) with z-axis corresponding with the axis of symmetry; r is the radial distance from the z axis, and θ is the polar angle in a plane perpendicular to the z axis. For azimuthally symmetric electron equilibria ($\partial/\partial\theta=0$ and $\partial/\partial z=0$) characterized by $n_e^0(r)$ and $\underset{\sim}{V}_e^0(\underset{\sim}{x})=V_{e\theta}^0(r)\hat{\underset{\sim}{e}}_\theta$, it is straightforward to show from Eq. (2) that the functional form of electron density profile $n_e^0(r)$ can be specified arbitrarily. Moreover, the deviation from equilibrium charge neutrality produces a radial electric field $E_r^0(r)=-\partial\phi^0/\partial r$ that influences the azimuthal motion of the electron fluid. It follows from Eq. (1) that equilibrium force balance in the radial direction can be expressed as $-m_e V_{e\theta}^{02}(r)/r=-eE_r^0(r)-eV_{e\theta}^0(r)B_0/c$, or equivalently

$$\omega_e^2-\omega_{ce}\omega_e+\omega_E\omega_{ce} = 0 \ , \tag{5}$$

where $\omega_{ce}=eB_0/m_e c$ is the electron cyclotron frequency, $\omega_e(r)=V_{e\theta}^0(r)/r$ is the angular velocity of an electron fluid element, and $\omega_E(r)$ is the angular $\underset{\sim}{E}^0\times\underset{\sim}{B}_0$ frequency defined by

$$\omega_E = -\frac{cE_r^0}{rB_0} = \frac{c}{rB_0}\frac{\partial\phi_0}{\partial r} \ . \tag{6}$$

We note from Eq. (5) that there are two allowed equilibrium values of $\omega_e(r)$. Solving Eq. (5) for $\omega_e(r)$ gives

$$\omega_e = \omega_e^{\pm} \equiv \frac{\omega_{ce}}{2}\left\{1 \pm \left(1 - \frac{4\omega_E}{\omega_{ce}}\right)^{1/2}\right\} \quad , \tag{7}$$

where the upper sign ($\omega_e=\omega_e^+$) corresponds to a "fast" rotational equilibrium, and the lower sign ($\omega_e=\omega_e^-$) corresponds to a "slow" rotational equilibrium. Evidently, in the limit of weak radial electric field with $|\omega_E| \lesssim \omega_{ce}$, it follows from Eq. (7) that $\omega_e^+ \simeq \omega_{ce}$ and $\omega_e^- \simeq \omega_E$.

For the ions, any distribution function $f_i^0(\underset{\sim}{x},\underset{\sim}{v})$ that is a function of the single-particle constants of the motion in the equilibrium fields is a solution to the steady-state ($\partial/\partial t=0$) ion Vlasov equation. For present purposes, we consider the class of rigid-rotor ion Vlasov equilibria described by

$$f_i^0 = f_i^0(H_\perp - \omega_i P_\theta, v_z) \quad , \tag{8}$$

where ω_i=const., v_z is the axial velocity, $H_\perp$ is the perpendicular energy

$$H_\perp = \frac{m_i}{2}(v_r^2+v_\theta^2) + e\phi^0(r) \quad , \tag{9}$$

P_θ is the canonical angular momentum

$$P_\theta = m_i r(v_\theta + r\omega_{ci}/2) \quad , \tag{10}$$

and $\omega_{ci}=eB_0/m_ic$ is the ion cyclotron frequency. Once the functional form of $f_i^0(H_\perp-\omega_iP_\theta, v_z)$ is specified, the equilibrium electrostatic potential $\phi^0(r)$ can be determined self-consistently from the steady-state Poisson equation

$$\frac{1}{r}\frac{\partial}{\partial r}\, r\, \frac{\partial \phi^0}{\partial r} = 4\pi e\left[\int d^3v f_i^0(H_\perp - \omega_i P_\theta, v_z) - n_e^0(r)\right] , \tag{11}$$

where $\int d^3v f_i^0 = n_i^0(r)$ is the equilibrium ion density.

An important feature of equilibrium distribution functions that depend on $H_\perp$ and P_θ exclusively through the linear combination $H_\perp - \omega_i P_\theta$ is that the mean azimuthal motion corresponds to a rigid rotation with angular velocity $\omega_i = \text{const}$. Defining the mean azimuthal velocity of the ions by $V_{i\theta}^0(r) = (\int d^3v v_\theta f_i^0)/(\int d^3v f_i^0)$, it is straightforward to show from Eqs. (8)-(10) that $V_{i\theta}^0(r) = \omega_i r$ for the class of ion equilibria described by Eq. (8). In the equilibrium and stability analysis that follows, it is useful to introduce perpendicular velocity variables appropriate to the rotating frame of the ions. Defining

$$\begin{aligned} V_x &= v_x + \omega_i y , \\ V_y &= v_y - \omega_i x , \end{aligned} \tag{12}$$

(or equivalently $V_r = v_r$ and $V_\theta = v_\theta - \omega_i r$), it is straightforward to show from Eqs. (9) and (10) that

$$H_\perp - \omega_i P_\theta = \frac{m_i}{2} V_\perp^2 + \psi(r) , \tag{13}$$

where $V_\perp^2 = V_x^2 + V_y^2 = V_r^2 + V_\theta^2$, and $\psi(r)$ is defined by

$$\psi(r) = e\phi^0(r) - \frac{m_i}{2}(\omega_i^2 + \omega_i \omega_{ci}) r^2 \tag{14}$$

Note in Eq. (13) that $m_i V_\perp^2/2$ is the perpendicular kinetic energy in a frame of reference rotating with angular velocity ω_i, and $\psi(r)$ is the effective potential in the rotating frame. Substituting Eq. (13) into Eq. (8), the equilibrium ion density profile $n_i^0(r) = \int d^3v f_i^0$ can be expressed as

$$n_i^0(r) = 2\pi \int_0^\infty dV_\perp V_\perp \int_{-\infty}^\infty dv_z f_i^0 \left(\frac{m_i}{2} V_\perp^2 + \psi(r),\ v_z \right) . \qquad (15)$$

Moreover, it can also be shown that the equilibrium pressure tensor in the plane perpendicular to $\hat{e}_z$ is isotropic with perpendicular pressure $P_{i\perp}^0(r)=n_i^0(r)T_{i\perp}^0(r)$ given by

$$n_i^0(r)T_{i\perp}^0(r) = 2\pi \int_0^\infty dV_\perp V_\perp \int_{-\infty}^\infty dv_z \frac{m_i}{2} V_\perp^2 f_i^0 \left(\frac{m_i}{2} V_\perp^2 + \psi(r),\ v_z \right). \qquad (16)$$

Equation (16), in effect, determines the perpendicular ion temperature profile $T_{i\perp}^0(r)$ in terms of the equilibrium distribution function f_i^0.

2.C Sharp-Boundary Equilibrium

The formalism outlined in Sec. 2.B can be used to investigate equilibrium properties for a broad class of electron density profiles $n_e^0(r)$ and ion distribution functions $f_i^0(H_\perp-\omega_i P_\theta, v_z)$. For purposes of analytic simplification in the stability analysis in Sec. 3.B, we specialize to the case of a sharp-boundary equilibrium (Fig. 2) in which the electrons have a rectangular density profile, i.e.,

$$n_e^0(r) = \begin{cases} n_0=\text{const.} , & 0<r<R_p , \\ 0 , & R_p<r<R_c . \end{cases} \qquad (17)$$

In Eq. (17), R_p denotes the radius of the plasma column, and $r=R_c$ is the radial location of a grounded conducting wall. For the ion equilibrium, we make that particular choice of f_i^0 that also gives a rectangular density profile, i.e.,

$$f_i^0 = \frac{fn_0 m_i}{2\pi} \delta(H_\perp-\omega_i P_\theta-\hat{T}_i) G(v_z) , \qquad (18)$$

where f and $\hat{T}_i$ are positive constants, and $G(v_z)$ is the parallel velocity distribution with normalization $\int_{-\infty}^\infty dv_z G(v_z)=1$. Substituting

Eq. (18) into Eq. (15), it is straightforward to show that the ion density profile can be expressed as

$$n_i^0(r) = \begin{cases} fn_0 = \text{const.} , & \psi(r) < \hat{T}_i , \\ 0 , & \psi(r) > \hat{T}_i . \end{cases} \tag{19}$$

In the region where the electron and ion densities are constant [Eqs. (17) and (19)], the solution to the equilibrium Poisson equation (11) corresponds to the parabolic potential

$$\phi^0(r) = \frac{m_i}{2e} \omega_E \omega_{ci} r^2 , \tag{20}$$

where $\phi^0(r=0)=0$ has been assumed, and

$$\omega_E = \frac{2\pi n_0 ec}{B_0} (1-f) = - \frac{c}{B_0 r} \frac{\partial \phi^0}{\partial r} = \text{const.} \tag{21}$$

is the $\underset{\sim}{E}^0 \times \underset{\sim}{B}_0$ rotation frequency. Substituting Eq. (20) into Eq. (14), the effective potential $\psi(r)$ can be expressed within the plasma column as

$$\psi(r) = \frac{1}{2} m_i \Omega^2 r^2 , \tag{22}$$

where Ω^2 is defined by

$$\Omega^2 = \omega_E \omega_{ci} - \omega_i^2 - \omega_i \omega_{ci} = (\omega_i - \omega_i^+)(\omega_i^- - \omega_i) \tag{23}$$

and $\omega_i^{\pm}$ is defined in Eq. (31). We note from Eqs. (17), (19) and (22) that the electron and ion density profiles precisely overlap with a common radius R_p (Fig. 2) provided $\psi(R_p)=\hat{T}_i$, i.e., provided

$$\hat{T}_i = \frac{m_i}{2} \Omega^2 R_p^2 , \tag{24}$$

which relates $\hat{T}_i$ and the radius R_p of the plasma column. Making use of Eqs. (22) and (24), the ion density profile in Eq. (19) becomes

$$n_i^0(r) = \begin{cases} fn_0 & , \quad 0<r<R_p \ , \\ 0 & , \quad R_p<r<R_c \ . \end{cases} \tag{25}$$

Comparing Eqs. (17) and (25), it is evident that $n_i^0(r)=fn_e^0(r)$, where f=const.=fractional charge neutralization.

We make use of Eqs. (16), (18), (22) and (24) to evaluate the perpendicular ion temperature profile $T_{i\perp}^0(r)$. Some straightforward algebra gives

$$T_{i\perp}^0(r) = \hat{T}_i[1-r^2/R_p^2] \tag{26}$$

for $0<r<R_p$. Note that $T_{i\perp}^0(r)$ is a maximum ($\hat{T}_i$) for r=0, and decreases to zero at the edge of the plasma column ($r=R_p$). For future reference, it is useful to introduce the ion diamagnetic frequency defined by $\omega_{di}=(c/eB_0n_i^0r)(\partial/\partial r)(n_i^0T_{i\perp}^0)$. Making use of Eqs. (25) and (26), we find

$$\omega_{di} = -\frac{\hat{T}_i c}{eB_0}\frac{2}{R_p^2} = \text{const.} \tag{27}$$

Substituting Eqs. (23) and (24) into Eq. (27) readily gives

$$\omega_i^2+\omega_i\omega_{ci} = \omega_{ci}(\omega_E+\omega_{di}) \ , \tag{28}$$

which relates the (constant) frequencies ω_i, ω_{ci}, ω_E and ω_{di}. Equation (28) is simply a statement of radial force balance (of centrifugal, magnetic, electric and pressure gradient forces) on an ion fluid element for the choice of equilibrium distribution function in Eq. (18). Equation (28) is a useful relation since it indicates that the angular rotation velocity ω_i cannot be specified independently of ω_{ci}, ω_E and ω_{di}. For example, zero mean rotation of the ions ($\omega_i=0$) is consistent only if $\omega_E=-\omega_{di}$, which corresponds to an exact balance

of electric and pressure gradient forces on an ion fluid element. On the other hand, for complete charge neutralization with f=1 and $\omega_E=0$, it follows from Eq. (28) that $\omega_i^2+\omega_i\omega_{ci}=\omega_{ci}\omega_{di}$. If (for example) the inequality $\omega_{di}^2<<\omega_{ci}^2$ is also satisfied, then the two solutions for ω_i can be approximated by $\omega_i=\omega_{di}$ and $\omega_i=-\omega_{ci}$, which correspond to "slow" and "fast" rotational equilibria, respectively. Finally, for the rectangular density profiles prescribed by Eqs. (17) and (25), it should be noted from Eqs. (7) and (21) that the mean azimuthal motion of the electron fluid corresponds to a rigid rotation with $\omega_e=\omega_e^{\pm}=\text{const.}$

2.D Ion Trajectories for Sharp-Boundary Equilibrium

Of particular interest in the stability analysis in Sec. 3.B are the ion orbits in the equilibrium field configuration [see Eq. (20)]

$$\underset{\sim}{B}^0(\underset{\sim}{x}) = B_0\hat{\underset{\sim}{e}}_z \ ,$$

$$\underset{\sim}{E}^0(\underset{\sim}{x}) = E_r^0(r)\hat{\underset{\sim}{e}}_r = -\frac{m_i}{e}\omega_b^2(x\hat{\underset{\sim}{e}}_x+y\hat{\underset{\sim}{e}}_y) \ . \tag{29}$$

In Eq. (29), we have introduced the electrostatic bounce frequency ω_b defined by

$$\omega_b^2 = \omega_E\omega_{ci} = \frac{2\pi n_0 e^2}{m_i}(1-f) \ . \tag{30}$$

If electric forces dominate magnetic forces ($\omega_b^2>>\omega_{ci}^2$), then the perpendicular ion motion is simple harmonic at frequency ω_b. In general, however, the electric and magnetic forces may be comparable, and the subsequent analysis indicates that the perpendicular ion

motion is biharmonic at frequencies ω_i^+ and ω_i^-, where

$$\omega_i^{\pm} \equiv -\frac{\omega_{ci}}{2}\left[1 \pm \left(1+\frac{4\omega_b^2}{\omega_{ci}^2}\right)^{1/2}\right] \tag{31}$$

$$= -\frac{\omega_{ci}}{2}\left[1 \pm \left(1+\frac{4\omega_E}{\omega_{ci}}\right)^{1/2}\right].$$

The ion trajectories required in the stability analysis satisfy

$$\frac{d\underset{\sim}{x}'}{dt'} = \underset{\sim}{v}' \ , \tag{32}$$

$$\frac{d\underset{\sim}{v}'}{dt'} = \frac{e}{m_i}\left(\underset{\sim}{E}^0(\underset{\sim}{x}') + \frac{\underset{\sim}{v}'\times B_0\hat{e}_z}{c}\right) \ ,$$

where $\underset{\sim}{x}'(t'=t)=\underset{\sim}{x}$ and $\underset{\sim}{v}'(t'=t)=\underset{\sim}{v}$. Substituting Eq. (29) into Eq. (32), we find

$$z' = z+v_z(t'-t) \tag{33}$$

and

$$\frac{d^2}{dt'^2}x'(t') = -\omega_b^2 x'(t') + \omega_{ci}\frac{d}{dt'}y'(t') \ ,$$

$$\frac{d^2}{dt'^2}y'(t') = -\omega_b^2 y'(t') - \omega_{ci}\frac{d}{dt'}x'(t') \ . \tag{34}$$

Equation (34) can be solved exactly to give the particle orbits in the plane perpendicular to $B_0\hat{e}_z$. In this regard, it is useful to make use of the velocity variables (V_x,V_y) in the rotating frame defined in Eq. (12). Moreover, we introduce the polar velocity variables $(V_\perp,\phi)$ in the rotating frame defined by

$$v_x+\omega_j y = V_x = V_\perp\cos\phi \ ,$$

$$v_y-\omega_j x = V_y = V_\perp\sin\phi \ . \tag{35}$$

In solving Eq. (34), we also make use of the fact that the Cartesian coordinates (x,y) are related to the polar coordinates (r,θ) by $x=r\cos\theta$ and $y=r\sin\theta$. Integrating Eq. (34) with respecr to t', and expressing the resulting solutions for x'(t') and y'(t') in terms of $(V_\perp,\phi)$ and (r,θ), we find

$$x'(\tau) = \frac{1}{\omega_i^+-\omega_i^-}\{V_\perp[\sin(\phi+\omega_i^+\tau)-\sin(\phi+\omega_i^-\tau)] + r(\omega_i-\omega_i^-)\cos(\theta+\omega_i^+\tau)-r(\omega_i-\omega_i^+)\cos(\theta+\omega_i^-\tau)\}\ , \tag{36}$$

and

$$y'(\tau) = \frac{1}{\omega_i^+-\omega_i^-}\{V_\perp[\cos(\phi+\omega_i^-\tau)-\cos(\phi+\omega_i^+\tau)] + r(\omega_i-\omega_i^-)\sin(\theta+\omega_i^+\tau) - r(\omega_i-\omega_i^+)\sin(\theta+\omega_i^-\tau)\}\ , \tag{37}$$

where $\tau=t'-t$, and $\omega_i^\pm$ is defined in Eq. (31). It is evident from Eqs. (36) and (37) that the perpendicular ion motion is biharmonic at frequencies ω_i^+ and ω_i^-. Shown in Fig. 3 are plots of ω_i^+/ω_{ci} and ω_i^-/ω_{ci} versus ω_b/ω_{ci}. Note that $\omega_i^\pm$ asymptotes at $\mp\omega_b-\omega_{ci}/2$ for $\omega_b^2>>\omega_{ci}^2$. In this limit, the ions are effectively unmagnetized and exhibit simple harmonic motion at frequency ω_b in the electrostatic potential $\phi^0(r)=(m_i/2e)\omega_b^2r^2$.

3. ELECTROSTATIC STABILITY PROPERTIES

3.A General Eigenavlue Equation

In this section, we linearize Eqs. (1)-(4) assuming electrostatic perturbations about the general class of axisymmetric equilibria described by $f_i^0 = f_i^0(H_\perp - \omega_i P_\theta, v_z)$ [Eq. (6)] and arbitrary electron density profile $n_e^0(r)$ (see Sec. 3.B). As indicated in the introduction, the present analysis assumes flute perturbations with $\partial/\partial z = 0$, so that all perturbations have spatial dependence only on $\underset{\sim}{x}_\perp = (x,y)$, or equivalently $\underset{\sim}{x}_\perp = (r,\theta)$. In the electrostatic approximation, the perturbed electric field is $\delta\underset{\sim}{E}(\underset{\sim}{x}_\perp,t) = -\nabla_\perp \delta\phi(\underset{\sim}{x}_\perp,t)$, and Eqs. (1)-(4) can be linearized to give

$$\left(\frac{\partial}{\partial t} + \omega_e \frac{\partial}{\partial \theta}\right)\delta V_{er} - (-\omega_{ce} + 2\omega_e)\delta V_{e\theta} = \frac{e}{m_e}\frac{\partial}{\partial r}\delta\phi \ , \tag{38}$$

$$\left(\frac{\partial}{\partial t} + \omega_e \frac{\partial}{\partial \theta}\right)\delta V_{e\theta} + \left(-\omega_{ce} + \frac{1}{r}\frac{\partial}{\partial r}(r^2\omega_e)\right)\delta V_{er} = \frac{e}{m_e}\frac{1}{r}\frac{\partial}{\partial \theta}\delta\phi \ , \tag{39}$$

$$\left(\frac{\partial}{\partial t} + \omega_e \frac{\partial}{\partial \theta}\right)\delta n_e + \frac{1}{r}\frac{\partial}{\partial r}(r n_e^0 \delta V_{er}) + \frac{n_e^0}{r}\frac{\partial}{\partial \theta}\delta V_{e\theta} = 0 \ , \tag{40}$$

$$\left\{\frac{\partial}{\partial t} + \underset{\sim}{v}\cdot\frac{\partial}{\partial \underset{\sim}{x}_\perp} + \frac{e}{m_i}\left[\underset{\sim}{E}^0(\underset{\sim}{x}_\perp) + \frac{\underset{\sim}{v}\times B_0 \hat{\underset{\sim}{e}}_z}{c}\right]\cdot\frac{\partial}{\partial \underset{\sim}{v}}\right\}\delta f_i(\underset{\sim}{x}_\perp,\underset{\sim}{v},t)$$

$$= \frac{e}{m_i}[\nabla_\perp \delta\phi(\underset{\sim}{x}_\perp,t)]\cdot\frac{\partial}{\partial \underset{\sim}{v}} f_i^0(\underset{\sim}{x}_\perp,\underset{\sim}{v}) \ , \tag{41}$$

and

$$\left(\frac{1}{r}\frac{\partial}{\partial r}\, r\, \frac{\partial}{\partial r} + \frac{1}{r^2}\frac{\partial^2}{\partial \theta^2}\right)\delta\phi = -4\pi e\left(\int d^3v \delta f_i - \delta n_e\right) \ . \tag{42}$$

In Eqs. (38)-(42), $\delta\underset{\sim}{V}_e(\underset{\sim}{x}_\perp,t)$ is the perturbed electron fluid velocity, $\delta n_e(\underset{\sim}{x}_\perp,t)$ is the perturbed electron density, $\delta f_i(\underset{\sim}{x}_\perp,\underset{\sim}{v},t)$ is the perturbed ion distribution function, $\underset{\sim}{E}^0(\underset{\sim}{x}_\perp) = -(\partial\phi^0/\partial r)\hat{\underset{\sim}{e}}_r$ is the equilibrium radial

electric field, $\phi^0(r)$ satisfies the steady-state Poisson equation (11), and $\omega_e(r)$ is the equilibrium angular velocity defined in Eq. (7).

To simplify the right-hand side of Eq. (41), use is made of $\partial H_\perp/\partial \underset{\sim}{v} = m_i \underset{\sim}{v}_\perp$ [Eq. (9)], $\partial P_\theta/\partial \underset{\sim}{v} = m_i r \hat{\underset{\sim}{e}}_\theta$ [Eq. (10)], where $\hat{\underset{\sim}{e}}_\theta$ is a unit vector in the θ-direction, and $\partial f_i^0/\partial P_\theta = -\omega_i \partial f_i^0/\partial H_\perp$ [Eq. (8)]. The linearized Vlasov equation (41) becomes

$$\left\{ \frac{\partial}{\partial t} + \underset{\sim}{v} \cdot \frac{\partial}{\partial \underset{\sim}{x}_\perp} + \frac{e}{m_i} \left(\underset{\sim}{E}^0(\underset{\sim}{x}_\perp) + \frac{\underset{\sim}{v} \times B_0 \hat{\underset{\sim}{e}}_z}{c} \right) \cdot \frac{\partial}{\partial \underset{\sim}{v}} \right\} \delta f_i(\underset{\sim}{x}_\perp, \underset{\sim}{v}, t)$$
$$= e(\underset{\sim}{v}_\perp - \omega_i r \hat{\underset{\sim}{e}}_\theta) \cdot \nabla_\perp \delta\phi(\underset{\sim}{x}_\perp, t) \frac{\partial}{\partial H_\perp} f_i^0(H_\perp - \omega_i P_\theta, v_z) \ . \tag{43}$$

We substitute

$$\delta\phi(\underset{\sim}{x}_\perp, t) = \delta\hat{\phi}(\underset{\sim}{x}_\perp) \exp(-i\omega t), \quad \mathrm{Im}\omega > 0 \ ,$$

in the right-hand side of Eq. (43) and integrate from $t' = -\infty$ to $t' = t$ using the method of characteristics. Neglecting initial perturbations and noting that v_z and $\partial f_i^0/\partial H_\perp$ are constant (independent of t') along a particle trajectory in the equilibrium field configuration, we find

$$\delta f_i(\underset{\sim}{x}_\perp, \underset{\sim}{v}, t) = e \frac{\partial f_i^0}{\partial H_\perp} \int_{-\infty}^{t} dt' \exp(-i\omega t')$$
$$\times \left\{ \underset{\sim}{v}'_\perp(t') \cdot \nabla'_\perp \delta\hat{\phi}[\underset{\sim}{x}'_\perp(t')] - \omega_i \frac{\partial}{\partial \theta'} \delta\hat{\phi}[\underset{\sim}{x}'_\perp(t')] \right\} , \tag{44}$$

where $\underset{\sim}{x}'_\perp(t')$ and $\underset{\sim}{v}'_\perp(t')$ are the perpendicular particle trajectories in the equilibrium fields $B_0 \hat{\underset{\sim}{e}}_z$ and $\underset{\sim}{E}^0(\underset{\sim}{x}_\perp) = -(\partial\phi^0/\partial r)\hat{\underset{\sim}{e}}_r$ [Eq. (32)], and $\phi^0(r)$ satisfies the general equilibrium Poisson equation (11). Making use of $\underset{\sim}{v}'_\perp \cdot \nabla'_\perp \delta\hat{\phi}(\underset{\sim}{x}'_\perp) = (d/dt')\delta\hat{\phi}(\underset{\sim}{x}'_\perp)$ to integrate by parts with respect to t', and changing variables to $\tau = t' - t$, Eq. (44) can also be expressed as

$$\delta f_i(\underset{\sim}{x}_\perp, \underset{\sim}{v}, t) = \delta\hat{f}_i(\underset{\sim}{x}_\perp, \underset{\sim}{v}) \exp(-i\omega t) \ ,$$

where

$$\delta\hat{f}_i(\underset{\sim}{x}_\perp,\underset{\sim}{v}) = \frac{e}{m_i}\frac{1}{v_\perp}\frac{\partial f_i^0}{\partial v_\perp}\left\{\delta\hat{\phi}(\underset{\sim}{x}_\perp) + \int_{-\omega}^{0} d\tau\exp(-i\omega\tau)\left(i\omega - \omega_i\frac{\partial}{\partial\theta'}\right)\delta\hat{\phi}(\underset{\sim}{x}'_\perp)\right\} . \tag{45}$$

In writing Eq. (45), we have made use of Eq. (13) to express

$$f_i^0(H_\perp - \omega_i P_\theta, v_z) = f_i^0\left(\frac{m_i}{2}v_\perp^2 + \psi(r),\ v_z\right) , \tag{46}$$

and hence $\partial f_i^0/\partial H_\perp = (m_i v_\perp)^{-1}\partial f_i^0/\partial v_\perp$, where $m_i v_\perp^2/2$ is the perpendicular kinetic energy in the rotating frame, and $\psi(r)$ is defined in Eq. (14).

We now assume perturbations of the form $\delta\hat{\phi}(\underset{\sim}{x}_\perp)=\hat{\phi}_\ell(r)\exp(i\ell\theta)$, $\delta\hat{n}_e(\underset{\sim}{x}_\perp)=\hat{n}_{e\ell}(r)\exp(i\ell\theta)$, etc., where ℓ is the azimuthal harmonic number. Some straightforward algebra that makes use of Eqs. (38)-(40) readily gives

$$4\pi e\hat{n}_{e\ell}(r) = -\frac{1}{r}\frac{\partial}{\partial r}\left\{r\frac{\omega_{pe}^2}{\nu_e^2}\frac{\partial}{\partial r}\hat{\phi}_\ell(r)\right\} + \frac{\ell^2}{r^2}\frac{\omega_{pe}^2}{\nu_e^2}\hat{\phi}_\ell(r) + \frac{\ell}{r}\hat{\phi}_\ell(r)\frac{1}{\omega-\ell\omega_e(r)}\frac{\partial}{\partial r}\left\{\frac{\omega_{pe}^2}{\nu_e^2}(-\omega_{ce}+2\omega_e)\right\} , \tag{47}$$

where $\omega_{pe}^2(r)=4\pi n_e^0(r)e^2/m_e$, $\nu_e^2(r)$ is defined by

$$\nu_e^2(r) = (\omega_{ce}-2\omega_e)\left\{\omega_{ce} - \frac{1}{r}\frac{\partial}{\partial r}(r^2\omega_e)\right\} - (\omega-\ell\omega_e)^2 , \tag{48}$$

and $\omega_e(r)$ is determined from Eqs. (7) and (11). Moreover, substituting Eqs. (45) and (47) into Eq. (42), the linearized Poisson equation can be expressed as

$$\frac{1}{r}\frac{\partial}{\partial r}\left\{r\left(1+\frac{\omega_{pe}^2}{\nu_e^2}\right)\frac{\partial}{\partial r}\hat{\phi}(r)\right\} - \frac{\ell^2}{r^2}\left(1+\frac{\omega_{pe}^2}{\nu_e^2}\right)\hat{\phi}(r) = \frac{\ell\hat{\phi}(r)}{r}\frac{1}{\omega-\ell\omega_e}\frac{\partial}{\partial r}\left\{\frac{\omega_{pe}^2}{\nu_e^2}(-\omega_{ce}+2\omega_e)\right\} \tag{49}$$

$$- \frac{4\pi e^2}{m_i} \int d^3v \, \frac{1}{V_\perp} \frac{\partial f_i^0}{\partial V_\perp} \left(\hat{\phi}(r) + i(\omega - \ell\omega_i) \int_{-\infty}^{0} d\tau \hat{\phi}(r') \exp[i\ell(\theta' - \theta) - i\omega\tau] \right) ,$$

where the abbreviated notation $\hat{\phi}(r) = \hat{\phi}_\ell(r)$ has been introduced in Eq. (49), and $r'(\tau=0)=r$ and $\theta'(\tau=0)=\theta$. Equation (49) is the eigenvalue equation that determines $\hat{\phi}(r)$ and the complex eigenfrequency ω for the class of ion equilibria described by Eq. (46) and general electron density profile $n_e^0(r)$ and angular velocity profile $\omega_e(r)$ consistent with Eqs. (7) and (11). In this regard, we note that the polar velocity variables $(V_\perp, \phi)$ defined in Eq. (35) are natural variables for the integrand in Eq. (49). Therefore, in the subsequent analysis of Eq. (49), we make use of

$$\int d^3v = \int_0^{2\pi} d\phi \int_0^{\infty} dV_\perp V_\perp \int_{-\infty}^{\infty} dv_z .$$

Moreover, it is convenient to introduce the phase-averaged (over ϕ) orbit integral $\hat{I}$ defined by

$$\hat{I} = i \int_0^{2\pi} \frac{d\phi}{2\pi} \int_{-\infty}^{0} d\tau \hat{\phi}(r') \exp[i\ell(\theta' - \theta) - i\omega\tau] . \tag{50}$$

3.B Eigenvalue Equation for Sharp-Boundary Equilibrium

We now specialize to the case where the equilibrium electron and ion density profiles are rectangular (Fig. 2), as discussed in Secs. 2.C and 2.D. The corresponding equilibrium ion distribution function is given by Eq. (18), which can be expressed in the equivalent form

$$f_i^0 = f \frac{n_0 m_i}{2\pi} \delta\left(\frac{m_i}{2} V_\perp^2 - \hat{T}_i \left(1 - \frac{r^2}{R_p^2} \right) \right) G(v_z) , \tag{51}$$

where use has been made of Eqs. (13), (14), (22) and (24).

Moreover, making use of Eq. (50) and $\partial n_e^0(r)/\partial r=-n_0\delta(r-R_p)$ [Eq. (17)], the eigenvalue equation (49) can be expressed as

$$\frac{1}{r}\frac{\partial}{\partial r}\left[r\left(1+\frac{\omega_{pe}^2}{\nu_e^2}\right)\frac{\partial}{\partial r}\hat{\phi}(r)\right]-\frac{\ell^2}{r^2}\left(1+\frac{\omega_{pe}^2}{\nu_e^2}\right)\hat{\phi}(r)$$

$$=\frac{\ell\hat{\phi}(r)}{r}\frac{\omega_{ce}-2\omega_e}{\omega-\ell\omega_e}\frac{\hat{\omega}_{pe}^2}{\nu_e^2}\delta(r-R_p) \tag{52}$$

$$-\frac{8\pi^2e^2}{m_i}\int_0^\infty dV_\perp V_\perp\int_{-\infty}^{\infty}dv_z\frac{1}{V_\perp}\frac{\partial f_i^0}{\partial V_\perp}[\hat{\phi}(r)+(\omega-\ell\omega_i)\hat{I}]\ ,$$

where

$$\nu_e^2(r)=(\omega_{ce}-2\omega_e)^2-(\omega-\ell\omega_e)^2=\text{const.}, \tag{53}$$

and

$$\omega_{pe}^2(r)=\begin{cases}\hat{\omega}_{pe}^2=\dfrac{4\pi n_0e^2}{m_e}=\text{const.}, & 0<r<R_p\ ,\\ 0\ , & R_p<r<R_c\end{cases} \tag{54}$$

Evidently, the angular frequencies ω_E [Eq. (21)], ω_b [Eq. (30)], ω_i^+ [Eq. (31)] and ω_e^+ [Eq. (7)] are constant (independent of r) for the case where the equilibrium electron and ion density profiles are rectangular (Fig. 2).

It is evident that the perturbed electron contribution to the right-hand side of Eq. (52) [the term proportional to $\partial n_e^0/\partial r=-n_0\delta(r-R_p)$ in Eq. (45)] is equal to zero except at the surface of the plasma column ($r=R_p$). Moreover, it can be shown that Eq. (52) supports a class of solutions in which the perturbed ion density [the term proportional to $\int d^3v\ V_\perp^{-1}\partial f_i^0/\partial V_\perp\ldots$ in Eq. (52)] is also equal to zero except at $r=R_p$. In this case, it follows from the linearized Poisson equation (52) that the electrostatic potential $\hat{\phi}(r)$ has the simple form

$$\hat{\phi}(r) = Ar^{\ell} \tag{55}$$

inside the plasma column ($0 \leq r < R_p$). In Eq. (55), A is a constant. The required orbit integral $\hat{I}$ [Eq. (50)] becomes

$$\hat{I} = iA \int_{-\infty}^{0} d\tau \exp[-i\ell\theta - i\omega\tau] \int_{0}^{2\pi} \frac{d\phi}{2\pi} [r'\exp(i\theta')]^{\ell}, \tag{56}$$

where we have interchanged the order of the τ and ϕ integrations. From Eqs. (36) and (37), we express

$$\begin{aligned} [r'\exp(i\theta')]^{\ell} &= [x'(\tau)+iy'(\tau)]^{\ell} \\ &= \frac{1}{(\omega_i^+ - \omega_i^-)^{\ell}} [i\alpha_1(\tau)V_{\perp}\exp(i\phi) + r\alpha_2(\tau)\exp(i\theta)]^{\ell} , \end{aligned} \tag{57}$$

where

$$\begin{aligned} \alpha_1(\tau) &= \exp(i\omega_i^-\tau) - \exp(i\omega_i^+\tau) , \\ \alpha_2(\tau) &= (\omega_i - \omega_i^-)\exp(i\omega_i^+\tau) - (\omega_i - \omega_i^+)\exp(i\omega_i^-\tau) , \end{aligned} \tag{58}$$

and $\omega_i^{\pm}$ is defined in Eq. (31). Substituting Eqs. (57) and (58) into Eq. (56), it is readily shown that

$$\begin{aligned} \hat{I} = i \frac{\hat{\phi}(r)}{(\omega_i^+ - \omega_i^-)^{\ell}} \int_{-\infty}^{0} d\tau \exp(-i\omega\tau) [(\omega_i - \omega_i^-)\exp(i\omega_i^+\tau) \\ - (\omega_i - \omega_i^+)\exp(i\omega_i^-\tau)]^{\ell} \end{aligned} \tag{59}$$

where $\hat{\phi}(r) = Ar^{\ell}$. An important feature of Eq. (59) is that the orbit integral $\hat{I}$ is independent of perpendicular energy $m_i V_{\perp}^2/2$. This is a consequence of the particularly simple form of $\hat{\phi}(r)$ within the plasma column [Eq. (55)].

Finally, after some straightforward algebra that utilizes Eq. (51), the ion velocity integral required in Eq. (52) can be evaluated

to give

$$2\pi \int_0^\infty dV_\perp V_\perp \int_{-\infty}^{\infty} dv_z \frac{1}{V_\perp} \frac{\partial f_i^0}{\partial V_\perp} = \frac{R_p}{(2\hat{T}_i/m_i)} \frac{\partial}{\partial r} n_i^0(r)$$

$$= -fn_0 \frac{R_p}{(2\hat{T}_i/m_i)} \delta(r-R_p) \tag{60}$$

Substituting Eqs. (59) and (60) into Eq. (52), the linearized Poisson equation for the sharp-boundary equilibrium discussed in Secs. 2.C and 2.D can be expressed as

$$\frac{1}{r}\frac{\partial}{\partial r}\left[r\left(1+\frac{\hat{\omega}_{pe}^2}{\nu_e^2}\right)\frac{\partial}{\partial r}\hat{\phi}(r)\right] - \frac{\ell^2}{r^2}\left(1+\frac{\hat{\omega}_{pe}^2}{\nu_e^2}\right)\hat{\phi}(r)$$

$$= \hat{\phi}(r)\left[\frac{\ell}{r}\frac{\hat{\omega}_{pe}^2}{\nu_e^2}\frac{\omega_{ce}^{-2\omega_e}}{\omega-\ell\omega_e} - \frac{\hat{\omega}_{pi}^2}{\hat{v}_i^2} R_p \Gamma_\ell(\omega)\right]\delta(r-R_p) \ , \tag{61}$$

where $\hat{v}_i^2 \equiv 2\hat{T}_i/m_i$, $\hat{\omega}_{pi}^2 \equiv 4\pi f n_0 e^2/m_i$, $\hat{\omega}_{pe}^2 \equiv 4\pi n_0 e^2/m_e$, $\omega_{ce} \equiv eB_0/m_e c$, $\omega_e = \omega_e^+$ is defined in Eq. (7) with $\omega_E \equiv (2\pi n_0 ec/B_0)(1-f) = (\hat{\omega}_{pe}^2/2\omega_{ce})(1-f)$ [Eq. (21)], ν_e^2 is defined in Eq. (53), and $\Gamma_\ell(\omega)$ is defined by

$$\Gamma_\ell(\omega) = -1 - \frac{i(\omega-\ell\omega_i)}{(\omega_i^+-\omega_i^-)^\ell}\int_{-\infty}^{0} d\tau \exp(-i\omega\tau)[(\omega_i-\omega_i^-)\exp(i\omega_i^+\tau)$$

$$- (\omega_i-\omega_i^+)\exp(i\omega_i^-\tau)]^\ell \tag{62}$$

$$= -1 + \left(\frac{\omega_i-\omega_i^+}{\omega_i^--\omega_i^+}\right)^\ell \sum_{m=0}^{\ell} \frac{\ell!}{m!(\ell-m)!} \frac{\omega-\ell\omega_i}{\omega-\ell\omega_i^- - m(\omega_i^+-\omega_i^-)} \left(\frac{\omega_i^--\omega_i}{\omega_i-\omega_i^+}\right)^m \ .$$

3.C Dispersion Relation for Sharp-Boundary Equilibrium

The right-hand side of the eigenvalue equation (61) is equal to zero except at the surface of the plasma column ($r=R_p$). Moreover,

the eigenfunction $\hat{\phi}(r)$ satisfies the vacuum Poisson equation, $r^{-1}(\partial/\partial r)[r\partial\hat{\phi}/\partial r]-(\ell^2/r^2)\hat{\phi}=0$, except at $r=R_p$. Therefore, the solution to Eq. (61) can be expressed as

$$\hat{\phi}_i(r)=Ar^{\ell} \quad , \quad 0 \leq r < R_p \quad , \tag{63}$$

inside the column, and

$$\hat{\phi}_o(r) = Ar^{\ell}\frac{[1-R_c^{2\ell}/r^{2\ell}]}{[1-R_c^{2\ell}/R_p^{2\ell}]} \quad , \quad R_p < r \leq R_c \quad , \tag{64}$$

in the vacuum region between the surface of the plasma column and the conducting wall. Note that $\hat{\phi}(r)$ is continuous at $r=R_p$, and that $\hat{\phi}_o(r=R_c)=0$. The dispersion relation that determines the complex eigenfrequency ω is determined by multiplying Eq. (61) by r and integrating from $R_p(1-\varepsilon)$ to $R_p(1+\varepsilon)$ with $\varepsilon\to 0_+$. This gives

$$\begin{aligned} R_p\left(\frac{\partial\hat{\phi}_o}{\partial r}\right)_{r=R_p} - R_p\left(1+\frac{\hat{\omega}_{pe}^2}{v_e^2}\right)\left(\frac{\partial\hat{\phi}_i}{\partial r}\right)_{r=R_p} \\ = \left(\ell\frac{\hat{\omega}_{pe}^2}{v_e^2}\frac{\omega_{ce}-2\omega_e}{\omega-\ell\omega_c} - \frac{\hat{\omega}_{pi}^2R_p^2}{\hat{v}_i^2}\Gamma_\ell(\omega)\right)\hat{\phi}(r=R_p) \quad . \end{aligned} \tag{65}$$

Substituting Eqs. (63) and (64) into Eq. (65) and rearranging terms gives the dispersion relation

$$\frac{1}{1-(R_p/R_c)^{2\ell}} = \frac{\hat{\omega}_{pe}^2}{2(\omega-\ell\omega_e)[(\omega-\ell\omega_e)-(\omega_{ce}-2\omega_e)]} + \frac{\hat{\omega}_{pi}^2R_p^2}{2\ell\hat{v}_i^2}\Gamma_\ell(\omega) \quad , \tag{66}$$

where $\Gamma_\ell(\omega)$ is defined in Eq. (62), $\omega_e=\omega_e^+$ is defined in Eq. (7) and use has been made of Eq. (53).

Equation (66) can be used to investigate the stability properties of a partially neutralized electron beam for a broad range of dimensionless parameters $\hat{\omega}_{pe}^2/\omega_{ce}^2$, f, etc. An important parameter that characterizes the strength of ion kinetic effects is the ratio of characteristic ion

Larmor radius ($\hat{r}_{Li}=\hat{v}_i/\omega_{ci}$) to radius of the plasma column (R_p). Making use of Eqs. (23) and (24), it is straightforward to show that

$$\frac{\hat{r}_{Li}^2}{R_p^2} = \frac{\hat{v}_i^2}{R_p^2\omega_{ci}^2} = \frac{\hat{\Omega}^2}{\omega_{ci}^2} = \frac{(\omega_i-\omega_i^+)(\omega_i^--\omega_i)}{\omega_{ci}^2} , \tag{67}$$

where $\omega_i^{\pm}$ is defined in Eq. (31). Evidently, the cold-ion limit (where the ion motion is laminar with $r_{Li}^2 \ll R_p^2$) corresponds to ion rotation velocities that satisfy $\omega_i \simeq \omega_i^-$ or $\omega_i \simeq \omega_i^+$. A careful examination of the expression for $\Gamma_\ell(\omega)$ [Eq. (62)] shows that

$$\lim_{\omega_i \to \omega_i^-} \left\{ \frac{\hat{\omega}_{pi}^2 R_p^2}{2\ell \hat{v}_i^2} \Gamma_\ell(\omega) \right\} = \frac{\hat{\omega}_{pi}^2}{2(\omega-\ell\omega_i^-)[(\omega-\ell\omega_i^-)+(\omega_{ci}+2\omega_i^-)]} \tag{68}$$

where use has been made of Eq. (67) and $\omega_i^- - \omega_i^+ = \omega_{ci}+2\omega_i^-$ [Eq. (31)]. Similarly, in the limit where $\omega_i \to \omega_i^+$, we obtain

$$\lim_{\omega_i \to \omega_i^+} \left\{ \frac{\hat{\omega}_{pi}^2 R_p^2}{2\ell \hat{v}_i^2} \Gamma_\ell(\omega) \right\} = \frac{\hat{\omega}_{pi}^2}{2(\omega-\ell\omega_i^+)[(\omega-\ell\omega_i^+)+(\omega_{ci}+2\omega_i^+)]} , \tag{69}$$

where $\omega_i^+ - \omega_i^- = \omega_{ci}+2\omega_i^+$. Therefore, making use of Eqs. (68) and (69), we find that the dispersion relation (66) in the limit of zero ion Larmor radius ($\hat{r}_{Li}^2/R_p^2 \to 0$) reduces to

$$\frac{1}{1-(R_p/R_c)^{2\ell}} = \frac{\hat{\omega}_{pe}^2}{2(\omega-\ell\omega_e)[(\omega-\ell\omega_e)-(\omega_{ce}-2\omega_e)]} + \frac{\hat{\omega}_{pi}^2}{2(\omega-\ell\omega_i)[(\omega-\ell\omega_i)+(\omega_{ci}+2\omega_i)]} , \tag{70}$$

where $\omega_i \simeq \omega_i^{\pm}$ [Eq. (31)]. Equation (70) is identical to the familiar dispersion relation[2,3] obtained within the framework of a cold two-fluid model. Throughout the remainder of this paper, Eq. (70) is referred to as the "reference dispersion relation" (RDR). In order to assess the influence of finite ion gyroradius on stability behavior, it will be useful to compare the stability information obtained from Eq. (66) with that obtained from Eq. (70).

4. STABILITY ANALYSIS

In this section, the linear dispersion relation (66) is solved numerically for the complex eigenfrequency $\omega=\omega_r+i\gamma$. In this regard, we assume throughout this section that the electron fluid is rotating in the slow equilibrium mode with

$$\begin{aligned}\omega_e = \bar{\omega}_e &= \frac{\omega_{ce}}{2}\left[1-\left(1-\frac{4\omega_E}{\omega_{ce}}\right)^{1/2}\right] \\ &= \frac{\omega_{ce}}{2}\left[1-\left(1-\frac{2\hat{\omega}_{pe}^2}{\omega_{ce}^2}(1-f)\right)^{1/2}\right],\end{aligned} \tag{71}$$

where use has been made of Eqs. (7) and (21). It is also assumed that the mean equilibrium motion of an ion fluid element corresponds to the slow rotation velocity defined by

$$\begin{aligned}\omega_i = \hat{\bar{\omega}}_i &\equiv -\frac{\omega_{ci}}{2}\left[1-\left(1+\frac{4(\omega_E+\omega_{di})}{\omega_{ci}}\right)^{1/2}\right] \\ &= -\frac{\omega_{ci}}{2}\left[1-\left(1+\frac{m_i}{m_e}\frac{2\hat{\omega}_{pe}^2}{\omega_{ce}^2}(1-f)-4\frac{\hat{r}_{Li}^2}{R_p^2}\right)^{1/2}\right].\end{aligned} \tag{72}$$

In obtaining Eq. (72), use has been made of Eqs. (27) and (28) to solve for $\omega_i=\hat{\bar{\omega}}_i$. For $\hat{r}_{Li}^2/R_p^2\ll 1$, we note from Eq. (72) that $\hat{\bar{\omega}}_i\simeq\bar{\omega}_i$, where $\bar{\omega}_i$ is the laminar rotation velocity defined in Eq. (31). Substituting Eqs. (71) and (72) into Eq. (66), the linear dispersion relation can be expressed as

$$\frac{1}{1-(R_p/R_c)^{2\ell}} = \frac{\hat{\omega}_{pe}^2}{2(\omega-\ell\bar{\omega}_e)[(\omega-\ell\bar{\omega}_e)-(\omega_{ce}-2\bar{\omega}_e)]} + \frac{\hat{\omega}_{pi}^2R_p^2}{2\ell\hat{v}_i^2}\Gamma_\ell(\omega), \tag{73}$$

where $\Gamma_\ell(\omega)$ is defined by [Eq. (62)]

$$\Gamma_\ell(\omega) = -1+\left(\frac{\hat{\bar{\omega}}_i-\omega_i^+}{\bar{\omega}_i-\omega_i^+}\right)^\ell \sum_{m=0}^{\ell}\frac{\ell!}{m!(\ell-m)!}\frac{\omega-\ell\hat{\bar{\omega}}_i}{\omega-\ell\bar{\omega}_i-m(\omega_i^+-\omega_i^-)}\left(\frac{\bar{\omega}_i-\hat{\bar{\omega}}_i}{\hat{\bar{\omega}}_i-\omega_i^+}\right)^m. \tag{74}$$

Moreover, in the laminar cold-fluid limit where $\hat{r}_{Li}^2/R_p^2=0$, $\omega_i=\omega_i^-$ and $\omega_e=\omega_e^-$, the reference dispersion relation (70) can be expressed as

$$\frac{1}{1-(R_p/R_c)^{2\ell}} = \frac{\hat{\omega}_{pe}^2}{2(\omega-\ell\omega_e^-)\left[(\omega-\ell\omega_e^-)-(\omega_{ce}-2\omega_e^-)\right]} + \frac{\hat{\omega}_{pi}^2}{2(\omega-\ell\omega_i^-)\left[(\omega-\ell\omega_i^-)+(\omega_{ci}+2\omega_i^-)\right]} \tag{75}$$

where ω_i^- and ω_e^- are defined in Eqs. (31) and (71), respectively. For the fundamental mode ($\ell=1$), we reiterate that the linear dispersion relation (73) is identical to the reference dispersion relation (75). Therefore, the Vlasov-fluid stability properties for $\ell=1$ are identical to those calculated from a macroscopic two-fluid model, and the growth rate is unaffected by the value of $\hat{r}_{Li}/R_p$.

Before proceeding with a detailed analysis of the dispersion relation (73) and comparison with the reference dispersion relation (75), it is useful to summarize the limitation on plasma parameters necessary for existence of the nonneutral equilibrium configuration. From Eqs. (71) and (72), we require

$$\frac{2\hat{\omega}_{pe}^2}{\omega_{ce}^2}(1-f) \leq 1 , \tag{76}$$

and

$$\frac{\hat{r}_{Li}^2}{R_p^2} \leq \frac{1}{4}\left(1+\frac{m_i}{m_e}\frac{2\hat{\omega}_{pe}^2}{\omega_{ce}^2}(1-f)\right) \tag{77}$$

for radial confinement of the equilibrium. The inequality in Eq. (76) assures that the (repulsive) space-charge force on an electron fluid element is weaker than the magnetic restoring force. Moreover, Eq. (77) is equivalent to the requirement that the pressure gradient force on an ion fluid element (in the outward direction, since $\partial\Upsilon_{i\perp}^0/\partial r<0$) is weaker than the confining electric and magnetic forces. In Fig. 4,

we make use of Eqs. (76) and (77) to illustrate the region of parameter space $(f,\hat{\omega}_{pe}^2/\omega_{ce}^2)$ corresponding to existence of allowed equilibria for $m_i/m_e=1836$ and several values of $\alpha=\hat{r}_{Li}/R_p$. Note that the equilibrium electron density can exceed the Brillouin flow limit $(\hat{\omega}_{pe}^2/\omega_{ce}^2=0.5)$ provided there is sufficient charge neutralization that $f\geq 1-0.5(\omega_{ce}^2/\hat{\omega}_{pe}^2)$. The uppermost curves in Fig. 4 are calculated from the inequality

$$f \leq 1 - \frac{\frac{m_e}{m_i}\left(4\frac{\hat{r}_{Li}^2}{R_p^2} - 1\right)}{2\hat{\omega}_{pe}^2/\omega_{ce}^2}, \tag{78}$$

which is equivalent to Eq. (77).

The growth rate $\gamma=\mathrm{Im}\omega$ and real oscillation frequency $\omega_r=\mathrm{Re}\omega$ have been obtained numerically from Eq. (73) for a broad range of plasma parameters f, $\hat{\omega}_{pe}^2/\omega_{ce}^2$ and $\hat{r}_{Li}/R_p$. We now summarize the essential features of these stability studies. The analysis is restricted to nonneutral proton-electron plasmas $(m_i/m_e=1836)$, and the growth rate and real frequency are measured in units of the lower hybrid frequency

$$\omega_{LH}=(\omega_{ce}\omega_{ci})^{1/2}.$$

Moreover, throughout the remainder of this section, it is assumed that

$$\frac{R_p}{R_c} = 0.5 .$$

A detailed study of the influence of the conducting wall location on stability behavior is summarized in Ref. 3 for $\hat{r}_{Li}/R_p=0$.

Stability boundaries in the parameter space $(f,\omega_{pe}^2/\omega_{ce}^2)$ are illustrated in Figs. 5-8 for several values of $\hat{r}_{Li}/R_p$ ranging from 0 to 2.5. In Fig. 5, the solid curves correspond to the stability

boundaries ($\gamma=0$) obtained from Eq. (73) [or Eq. (75)] for $\hat{r}_{Li}/R_p=0$, and several values of azimuthal harmonic number ℓ. For a given value of ℓ, the region of $(f,\hat{\omega}_{pe}^2/\omega_{ce}^2)$ parameter space <u>above</u> the curve corresponds to instability ($\gamma>0$), whereas the region of parameter space <u>below</u> the curve corresponds to stability ($\gamma=0$). For moderate plasma densities ($\hat{\omega}_{pe}^2/\omega_{ce}^2>0.01$, say), we note that the number of unstable modes increases rapidly as the fractional charge neutralization f is increased to values comparable with unity. In Fig. 6, the solid curves correspond to the stability boundaries obtained from Eq. (73) for $\hat{r}_{Li}/R_p=0.5$, and $\ell=2$, 4 and 10. It is important to note that the system is stable in the region of parameter space where the equilibrium space-charge field is weak [see the upper left-hand corner of Figs. 6(a)-6(c)]. Also note that the stable region of parameter space increases in area as the azimuthal mode number ℓ is increased [compare Figs. 6(a) and 6(c)]. In Figs. 7 and 8, the stability boundaries are illustrated for $\hat{r}_{Li}/R_p=1$ and $\hat{r}_{Li}/R_p=2.5$. Evidently, for such large values of $\hat{r}_{Li}/R_p$, the region of $(f,\hat{\omega}_{pe}^2/\omega_{ce}^2)$ parameter space corresponding to allowed equilibria becomes increasingly limited by the constraint in Eq. (78) [see also Fig. 4]. However, the qualitative features of the stability boundaries, and their dependence on mode number ℓ, are otherwise similar to Figs. 5 and 6.

The dependence of stability properties on fractional charge neutralization f is further illustrated in Figs. 9-11, where the normalized growth rate γ/ω_{LH} and oscillation frequency ω_r/ω_{LH} are plotted versus f for $\hat{\omega}_{pe}^2/\omega_{ce}^2=0.002$ (Figs. 9 and 10) and $\hat{\omega}_{pe}^2/\omega_{ce}^2=0.5$ (Fig. 11), and several values of mode number ℓ. We also assume $\hat{r}_{Li}/R_p=0$ in Fig. 9, and $\hat{r}_{Li}/R_p=0.5$ in Figs. 10 and 11. In Figs. 9(b), 10(b) and 11(b), ω_r/ω_{LH} is plotted only for the ranges of f

corresponding to instability ($\gamma>0$). Several features are noteworthy in Figs. 9 and 10. First, the number of unstable modes increases rapidly as f is increased. Second, for $\ell \geq 2$, the instability growth rate is significantly reduced by finite ion Larmor radius effects, particularly when the equilibrium self electric field is sufficiently weak. [For example, compare Figs. 10(a) and 9(a) with f approaching unity]. Third, for low beam densities, we note that the real frequency ω_r exhibits a nearly linear dependence on the fractional charge neutralization f [Figs. 9(b) and 10(b)].

The dependence of stability properties on beam density is illustrated in Fig. 12 where γ/ω_{LH} and ω_r/ω_{LH} are plotted versus $\hat{\omega}_{pe}^2/\omega_{ce}^2$ for f=0.5, $r_{Li}/R_p=0.5$ and several values of ℓ. As shown in Fig. 12(a), the absolute maximum growth rate ($\gamma_M \simeq 0.56\ \omega_{LH}$) for this choice of parameters occurs for $\ell=2$ and $\hat{\omega}_{pe}^2/\omega_{ce}^2=0.38$. The abscissa in Fig. 12 extends to $\hat{\omega}_{pe}^2/\omega_{ce}^2=1.0$ since physically allowed equilibria exist for $\hat{\omega}_{pe}^2/\omega_{ce}^2 \leq 0.5/(1-0.5)=1$ [Eq. (76) and Fig. 4].

Of considerable interest for experimental application is the stability behavior for specified values of f, $\hat{\omega}_{pe}^2/\omega_{ce}^2$ and $\hat{r}_{Li}/R_p$. Typical results are summarized in Figs. 13-15, where γ/ω_{LH} and ω_r/ω_{LH} are plotted versus mode number ℓ for $\hat{\omega}_{pe}^2/\omega_{ce}^2=0.01$ (Figs. 13 and 14), $\hat{\omega}_{pe}^2/\omega_{ce}^2=0.5$ (Fig. 15), $\hat{r}_{Li}/R_p=0$ (Fig. 13), $\hat{r}_{Li}/R_p=1.0$ (Figs. 14 and 15), and several values of fractional charge neutralization f. The graphical results are presented only for unstable modes with $\gamma>0$. For sufficiently low beam densities and large fractional charge neutralization ($\hat{\omega}_{pe}^2/\omega_{ce}^2=0.01$ and f=0.8 in Figs. 13 and 14), we note that finite ion Larmor radius effects reduces the instability growth rate and the number of unstable modes. For example, for $\hat{r}_{Li}/R_p=0$ and f=0.8, the absolute maximum growth rate ($\gamma_M=0.07\ \omega_{LH}$) occurs for $\ell=12$, and the system is

unstable for ℓ in the range $1 \leq \ell \leq 18$ [Fig. 13(a)]. On the other hand, for $\hat{r}_{Li}/R_p = 1.0$ and $f = 0.8$, the absolute maximum growth rate ($\gamma_M = 0.055\ \omega_{LH}$) occurs for $\ell = 9$, and the system is unstable for $1 \leq \ell \leq 14$ [Fig. 14(a)]. For high beam densities (Fig. 15), finite ion Larmor radius effects have a negligible influence on stability behavior (see also Fig. 11), although there is a substantial reduction in the number of unstable modes relative to the low-density case (Figs. 13 and 14).

5. CONCLUSIONS

In this paper, we have investigated the influence of finite ion Larmor radius effects on the ion resonance instability in a nonneutral plasma column. The equilibrium and stability analysis (Secs. 2-4) was carried out within the framework of a hybrid Vlasov-fluid model in which the ions are described by the Vlasov equation and the electrons are described as a macroscopic, cold fluid immersed in a uniform axial magnetic field $B_0\hat{e}_z$. Moreover, electrostatic stability properties were calculated for the case in which the equilibrium electron and ion density profiles are rectangular (Fig. 2) and the equilibrium ion distribution function is specified by Eq. (18). In circumstances where the perturbed ion density corresponds to a surface-charge perturbation (at $r=R_p$), a striking feature of the stability analysis is the fact that the required orbit integral $\hat{I}$ [Eq. (50)] can be evaluated in closed form [Eqs. (59) and (62)] for general values of the parameters $\hat{r}_{Li}/R_p$ and $(2\hat{\omega}_{pe}^2/\omega_{ce}^2)(1-f)$. In addition, the resulting eigenvalue equation (61) can be solved exactly to give the closed dispersion relation (66). A detailed numerical analysis of Eq. (66) was presented in Sec. 4, and it was shown that the growth rate of the ion resonance instability exhibits a very sensitive dependence on $\hat{r}_{Li}/R_p$, $\hat{\omega}_{pe}^2/\omega_{ce}^2$ and f. For example, finite ion Larmor radius effects can have a strong stabilizing influence for mode numbers $\ell \geq 2$ (see, for example, Figs. 10 and 14), particularly when the equilibrium self-electric field is weak ($\hat{\omega}_{pe}^2/\omega_{ce}^2 \ll 1$ or f close to unity). For the fundamental mode ($\ell=1$), however, stability properties are identical to those calculated from a macroscopic two-fluid model, and the growth rate is unaffected by the value of $\hat{r}_{Li}/R_p$.

ACKNOWLEDGMENTS

This research was supported by the National Science Foundation. The research by one of the authors (H.U.) was supported in part by the Office of Naval Research under auspices of the University of Maryland-Naval Research Laboratory Joint Program in Plasma Physics. One of us (R.C.D.) would also like to thank Professor K. Nishikawa and the Japan Society for the Promotion of Science for the opportunity to visit the University of Hiroshima, where part of this research was carried out.

REFERENCES

1. R. C. Davidson, Theory of Nonneutral Plasmas (W. A. Benjamin, Reading, Mass., 1974).
2. Loc. cit., p. 62.
3. R. C. Davidson and H. Uhm, "Influence of Strong Self Electric Fields on the Ion Resonance Instability in a Nonneutral Plasma Column", submitted for publication (1977).
4. R. H. Levy, J. D. Daugherty, and O. Buneman, Phys. Fluids 12, 2616 (1969).
5. D. G. Koshkarev and P. R. Zenkevich, Particle Accel. 3, 1 (1972).
6. D. A. D'Ippolito and R. C. Davidson, Phys. Fluids 18, 1507 (1975).
7. J. P. Freidberg, Phys. Fluids 15, 1102 (1972).
8. R. N. Sudan and M. Rosenbluth, Phys. Rev. Lett. 36, 972 (1976).
9. R. C. Davidson, Phys. Fluids 19, 1189 (1976).

FIGURE CAPTIONS

Fig. 1 Equilibrium configuration and coordinate system.

Fig. 2 Rectangular electron and ion density profiles [Eqs. (17) and (25)].

Fig. 3 Plots of ω_i^+/ω_{ci} and ω_i^-/ω_{ci} versus ω_b/ω_{ci} [Eq. (31)].

Fig. 4 Region of allowed equilibria [Eqs. (76) and (77)] in the parameter space $(f, \omega_{pe}^2/\omega_{ce}^2)$ for $m_i/m_e=1836$ and several values of $\alpha=\hat{r}_{Li}/R_p$.

Fig. 5 Stability boundaries [Eq. (75)] in the parameter space $(f, \omega_{pe}^2/\omega_{ce}^2)$ for $m_i/m_e=1836$, $R_p/R_c=0.5$, $\hat{r}_{Li}/R_p=0$, and several values of ℓ.

Fig. 6 Stability boundaries [Eq. (73)] in the parameter space $(f, \omega_{pe}^2/\omega_{ce}^2)$ for $m_i/m_e=1836$, $R_p/R_c=0.5$, $\hat{r}_{Li}/R_p=0.5$, and (a) $\ell=2$, (b) $\ell=4$ and (c) $\ell=10$.

Fig. 7 Stability boundaries [Eq. (73)] in the parameter space $(f, \omega_{pe}^2/\omega_{ce}^2)$ for $m_i/m_e=1836$, $R_p/R_c=0.5$, $\hat{r}_{Li}/R_p=1.0$, and several values of ℓ.

Fig. 8 Stability boundaries [Eq. (73)] in the parameter space $(f, \omega_{pe}^2/\omega_{ce}^2)$ for $m_i/m_e=1836$, $R_p/R_c=0.5$, $\hat{r}_{Li}/R_p=2.5$, and several values of ℓ.

Fig. 9 Plots of (a) growth rate γ and (b) real frequency ω_r versus f [Eq. (75)] for $\omega_{pe}^2/\omega_{ce}^2=0.002$, $m_i/m_e=1836$, $R_p/R_c=0.5$, $\hat{r}_{Li}/R_p=0$, and several values of ℓ.

Fig. 10 Plots of (a) growth rate γ and (b) real frequency ω_r versus f [Eq. (73)] for $\hat{\omega}_{pe}^2/\omega_{ce}^2=0.002$, $m_i/m_e=1836$, $R_p/R_c=0.5$, $\hat{r}_{Li}/R_p=0.5$, and several values of ℓ.

Fig. 11 Plots of (a) growth rate γ and (b) real frequency ω_r versus f [Eq. (73)] for $\hat{\omega}_{pe}^2/\omega_{ce}^2=0.5$, $m_i/m_e=1836$, $R_p/R_c=0.5$, $\hat{r}_{Li}/R_p=0.5$, and several values of ℓ.

Fig. 12 Plots of (a) growth rate γ and (b) real frequency ω_r versus $\hat{\omega}_{pe}^2/\omega_{ce}^2$ [Eq. (73)] for f=0.5, $m_i/m_e=1836$, $R_p/R_c=0.5$, $\hat{r}_{Li}/R_p=0.5$, and several values of ℓ.

Fig. 13 Plots of (a) growth rate γ and (b) real frequency ω_r versus ℓ [Eq. (75)] for $\hat{\omega}_{pe}^2/\omega_{ce}^2=0.01$, $m_i/m_e=1836$, $R_p/R_c=0.5$, $\hat{r}_{Li}/R_p=0$, and several values of f.

Fig. 14 Plots of (a) growth rate γ and (b) real frequency ω_r versus ℓ [Eq. (73)] for $\hat{\omega}_{pe}^2/\omega_{ce}^2=0.01$, $m_i/m_e=1836$, $R_p/R_c=0.5$, $\hat{r}_{Li}/R_p=1.0$, and several values of f.

Fig. 15 Plots of (a) growth rate γ and (b) real frequency ω_r versus ℓ [Eq. (73)] for $\hat{\omega}_{pe}^2/\omega_{ce}^2=0.5$, $m_i/m_e=1836$, $R_p/R_c=0.5$, $\hat{r}_{Li}/R_p=1.0$, and several values of f.

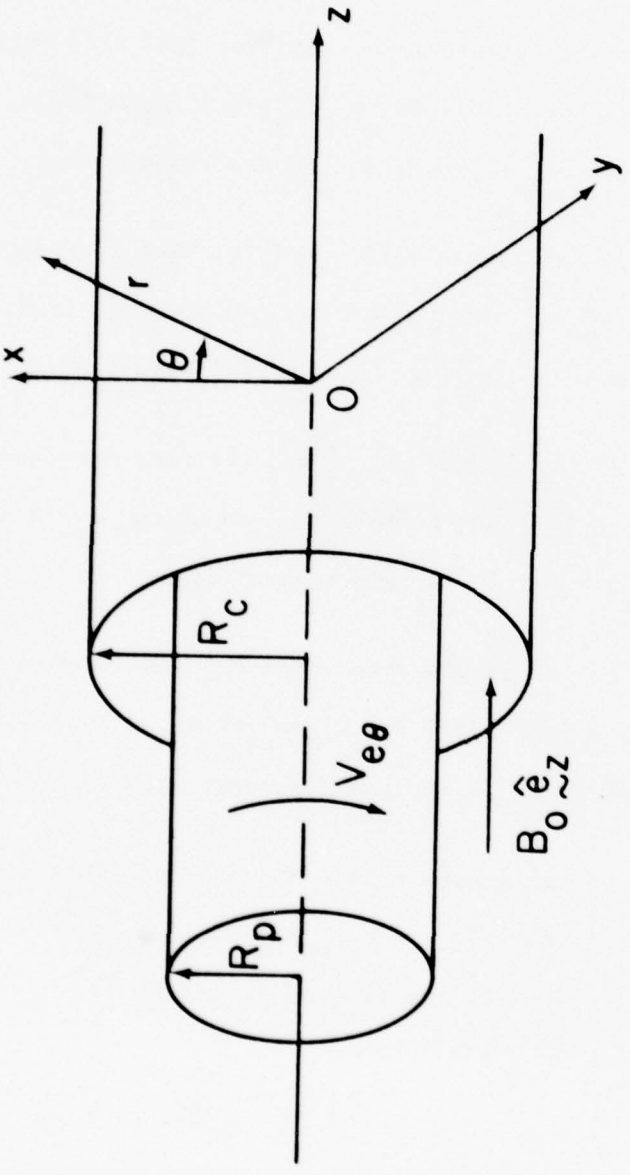

Fig. 1

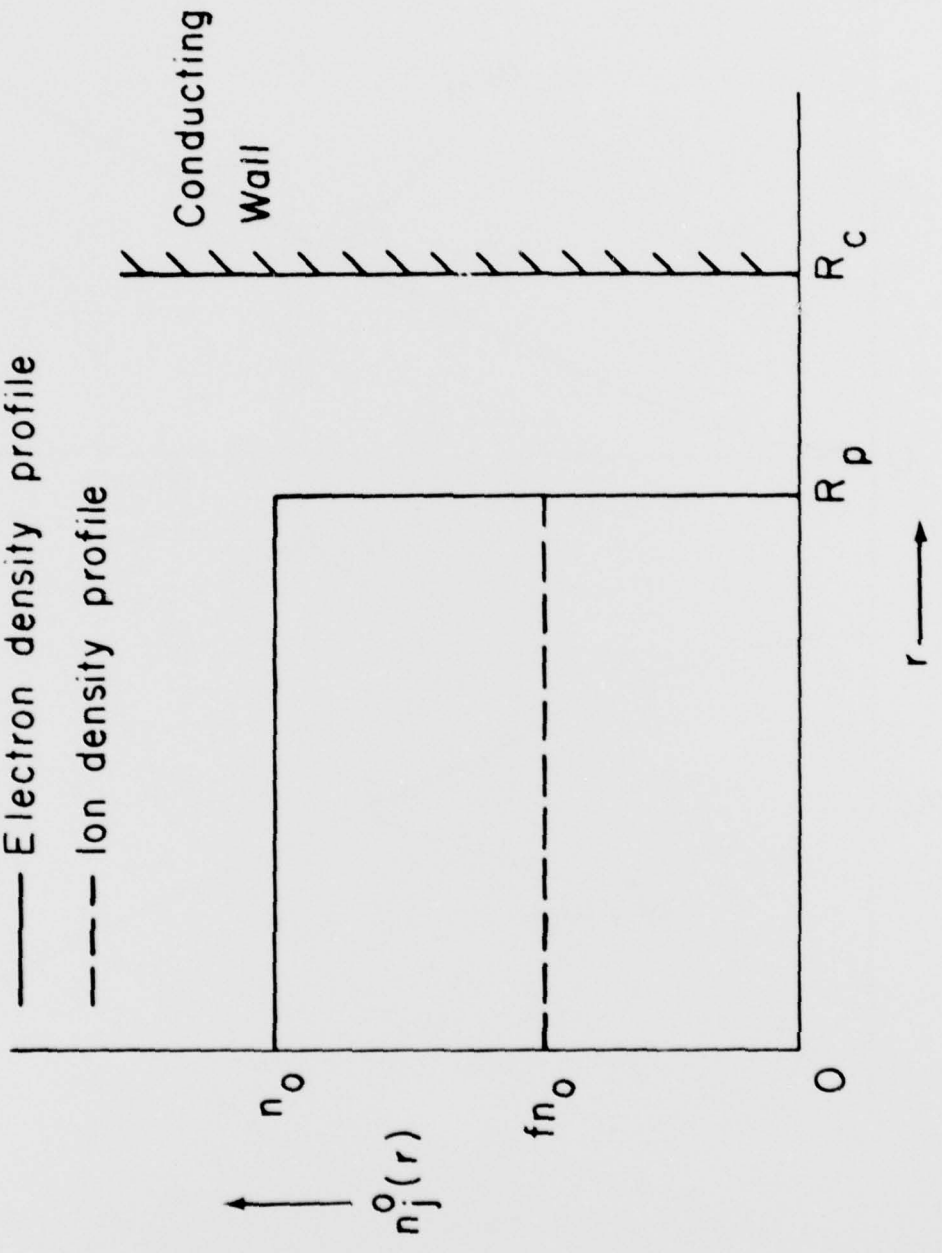
Electron density profile
Ion density profile
Conducting
Wall
R_c
R_p
r
n_o
fn_o
0
$n_j^o(r)$

Fig. 2

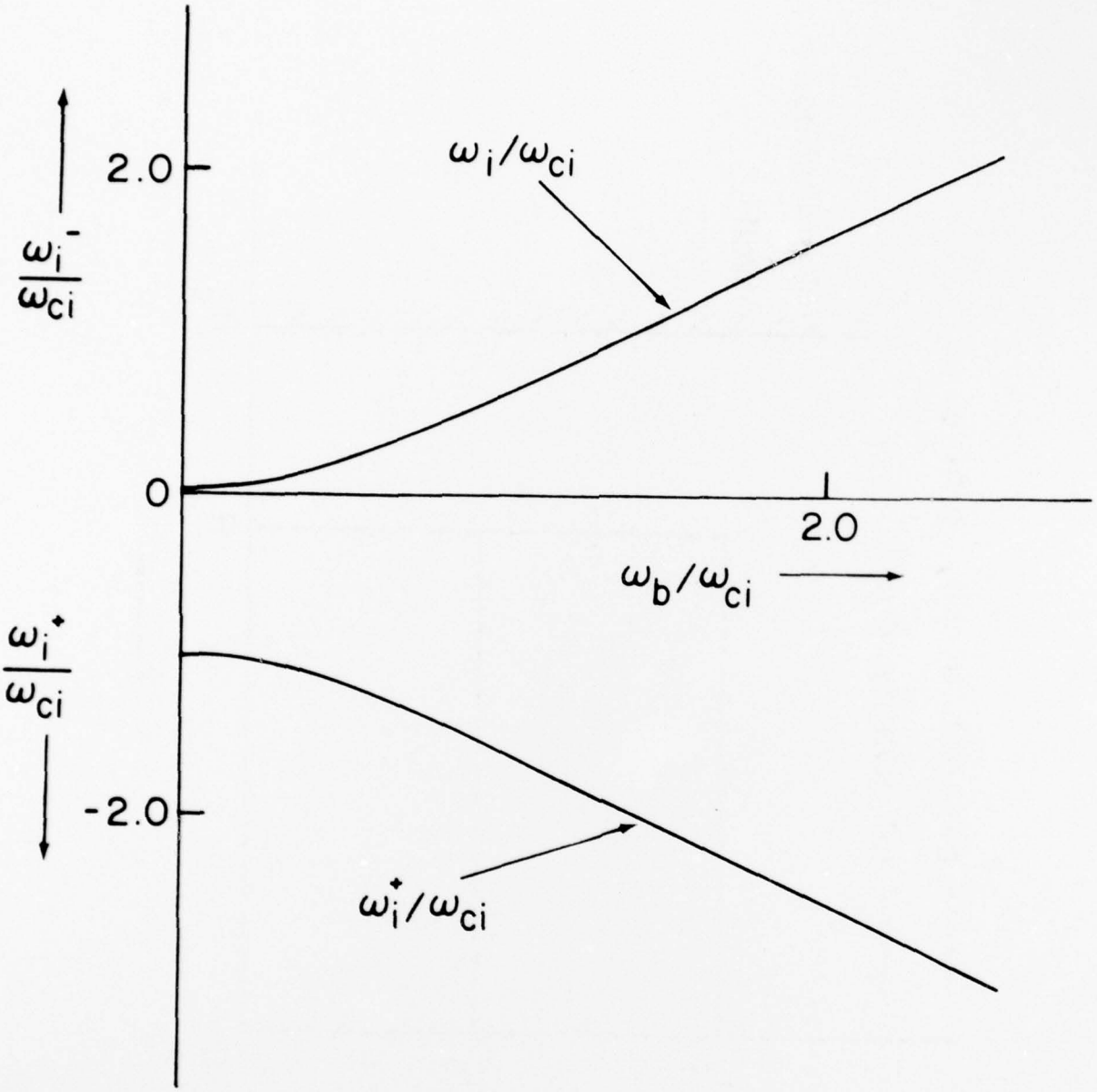
2.0
$\frac{\omega_i^-}{\omega_{ci}}$
ω_i/ω_{ci}
0
2.0
ω_b/ω_{ci}
$\frac{\omega_i^+}{\omega_{ci}}$
-2.0
ω_i^+/ω_{ci}

Fig. 3

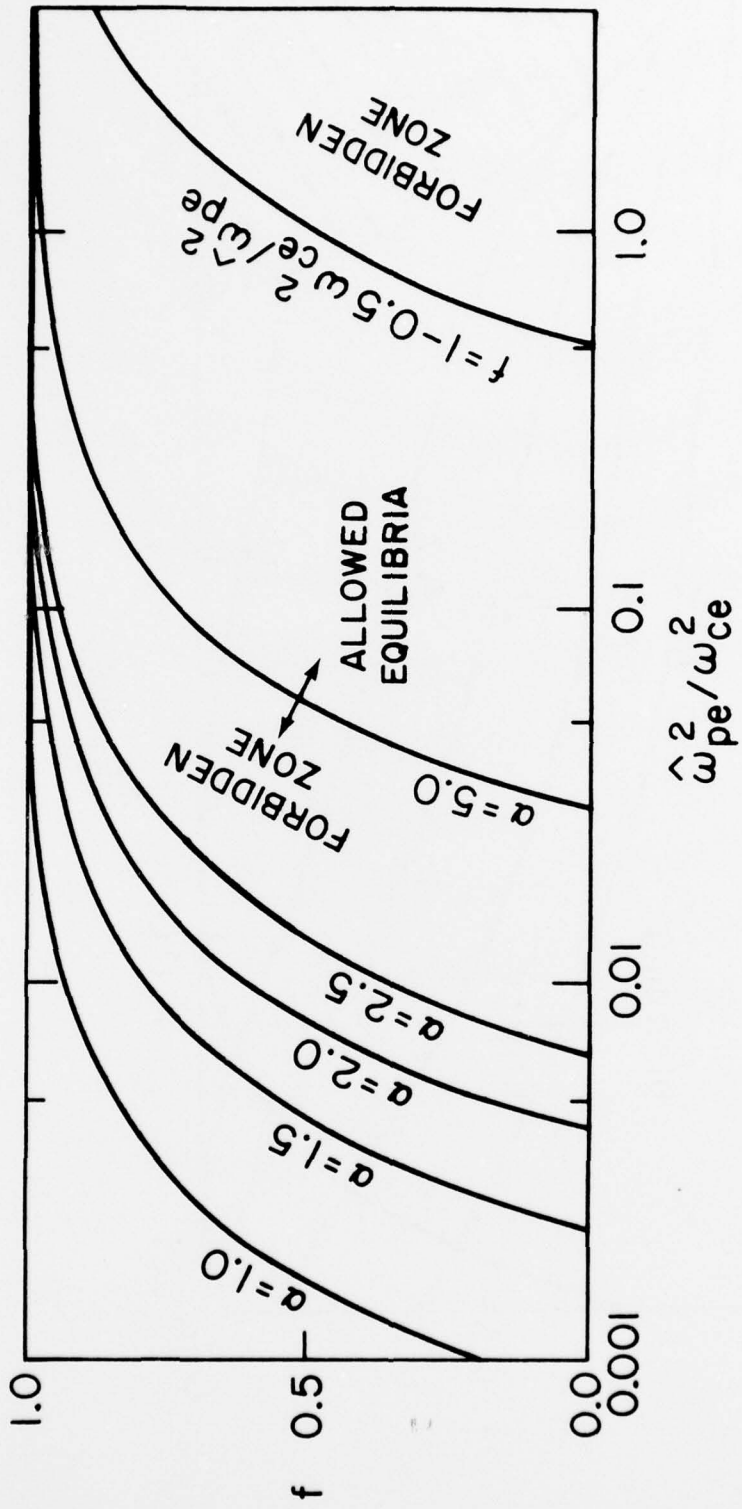
FORBIDDEN ZONE
$f = 1 - 0.5\omega_{ce}^2/\hat{\omega}_{pe}^2$
ALLOWED EQUILIBRIA
FORBIDDEN ZONE
$q = 5.0$
$q = 2.5$
$q = 2.0$
$q = 1.5$
$q = 1.0$
1.0
0.1
0.01
0.001
0.0
0.5
1.0
f
$\hat{\omega}_{pe}^2/\omega_{ce}^2$

Fig. 4

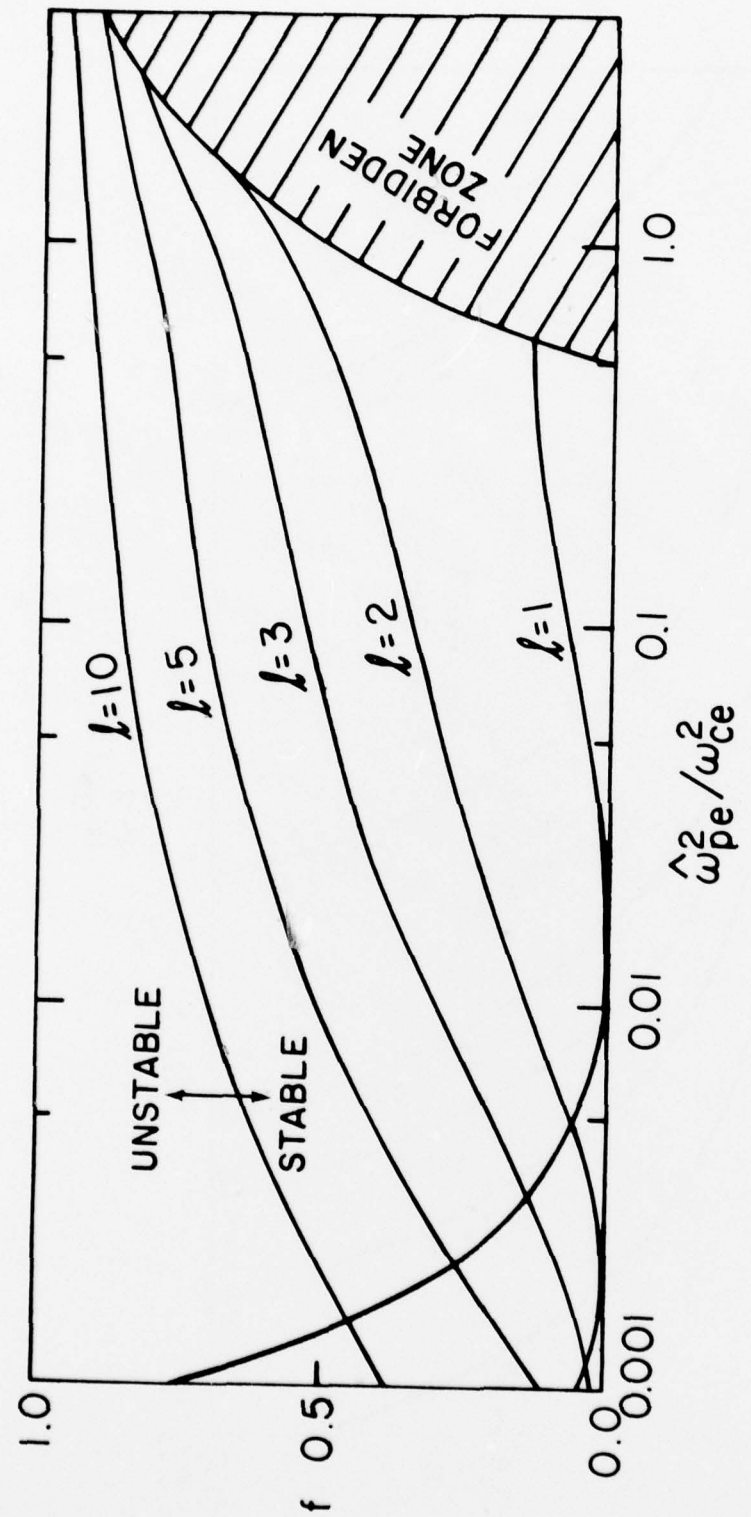
FORBIDDEN ZONE
UNSTABLE
STABLE
l=10
l=5
l=3
l=2
l=1
1.0
0.5
0.0
f
0.001
0.01
0.1
1.0
$\hat{\omega}^2_{pe}/\omega^2_{ce}$

Fig. 5

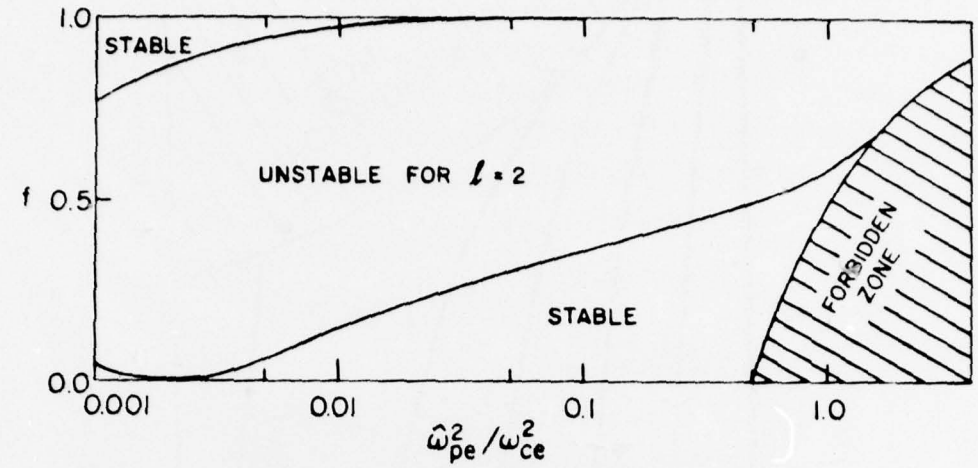
1.0
STABLE
UNSTABLE FOR ℓ = 2
f 0.5
STABLE
FORBIDDEN ZONE
0.0
0.001
0.01
0.1
1.0
$\hat{\omega}_{pe}^2/\omega_{ce}^2$

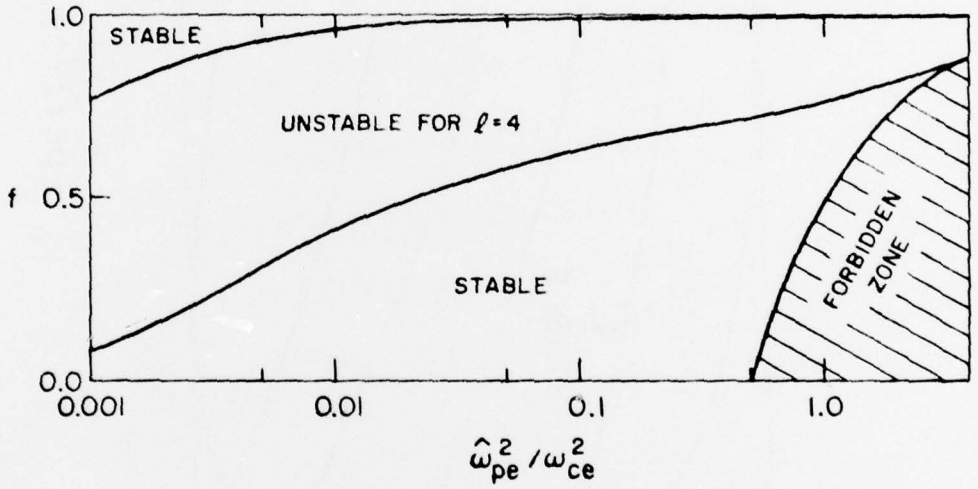
1.0
STABLE
UNSTABLE FOR ℓ=4
f 0.5
STABLE
FORBIDDEN ZONE
0.0
0.001
0.01
0.1
1.0
$\hat{\omega}_{pe}^2/\omega_{ce}^2$

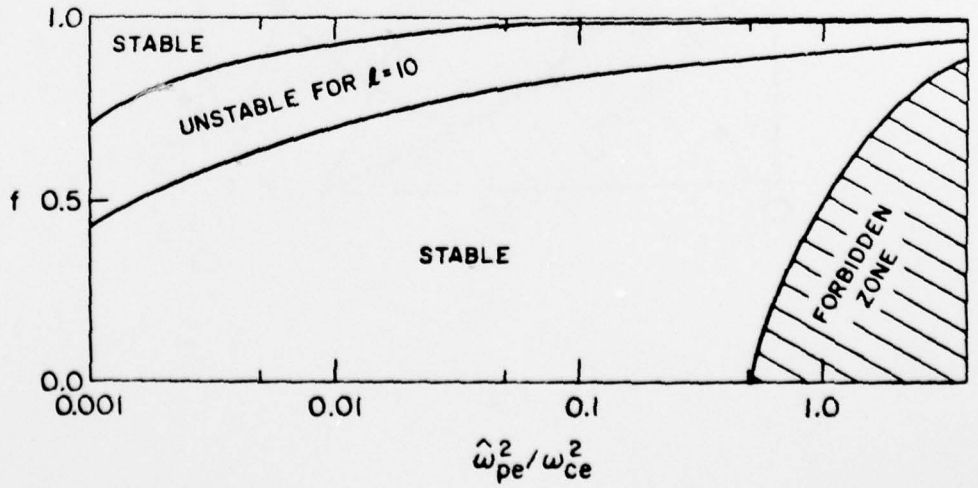
1.0
STABLE
UNSTABLE FOR ℓ=10
f 0.5
STABLE
FORBIDDEN ZONE
0.0
0.001
0.01
0.1
1.0
$\hat{\omega}_{pe}^2/\omega_{ce}^2$

Fig. 6

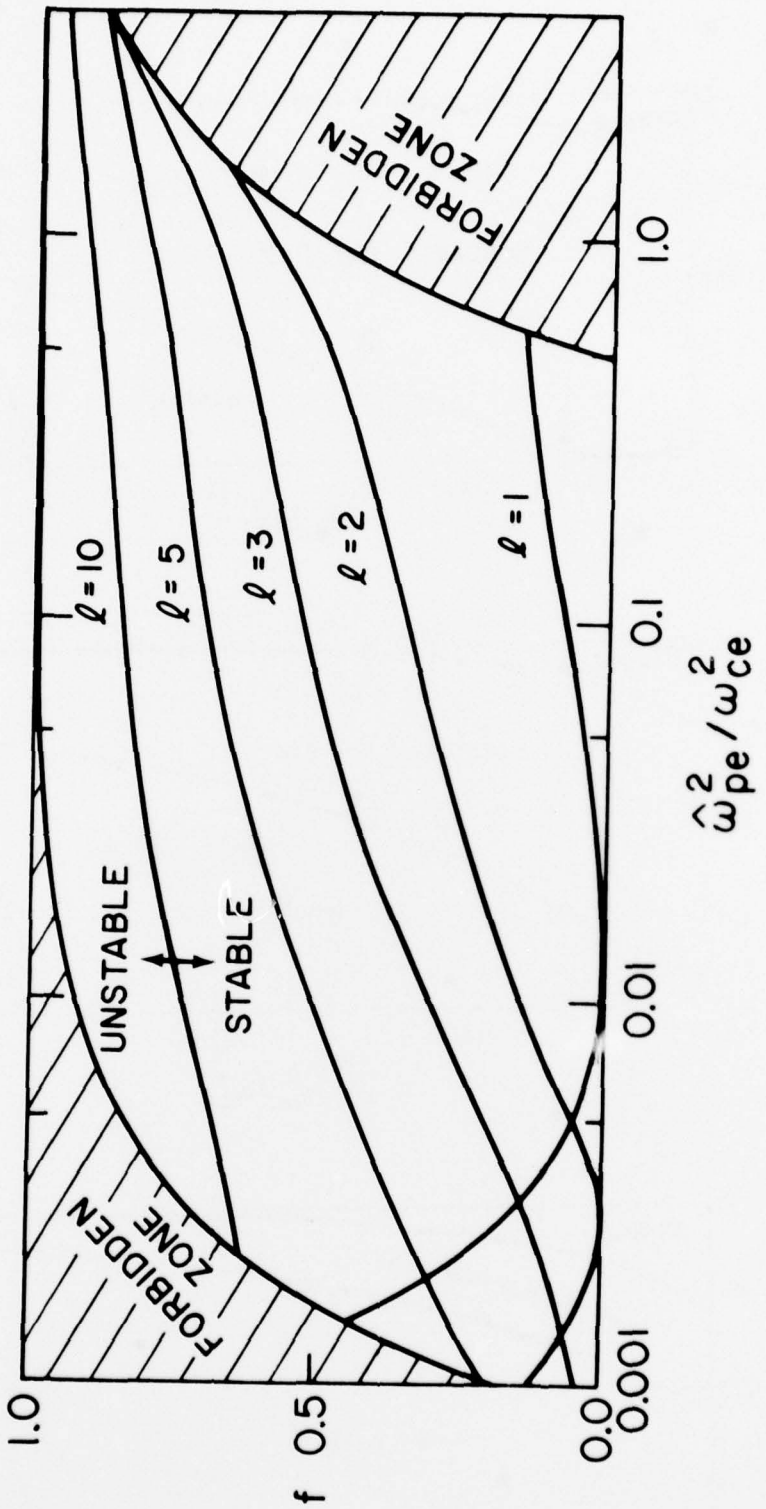
FORBIDDEN ZONE
FORBIDDEN ZONE
UNSTABLE
STABLE
ℓ=10
ℓ=5
ℓ=3
ℓ=2
ℓ=1
1.0
0.5
0.0
f
1.0
0.1
0.01
0.001
$\hat{\omega}^2_{pe}/\omega^2_{ce}$

Fig. 7

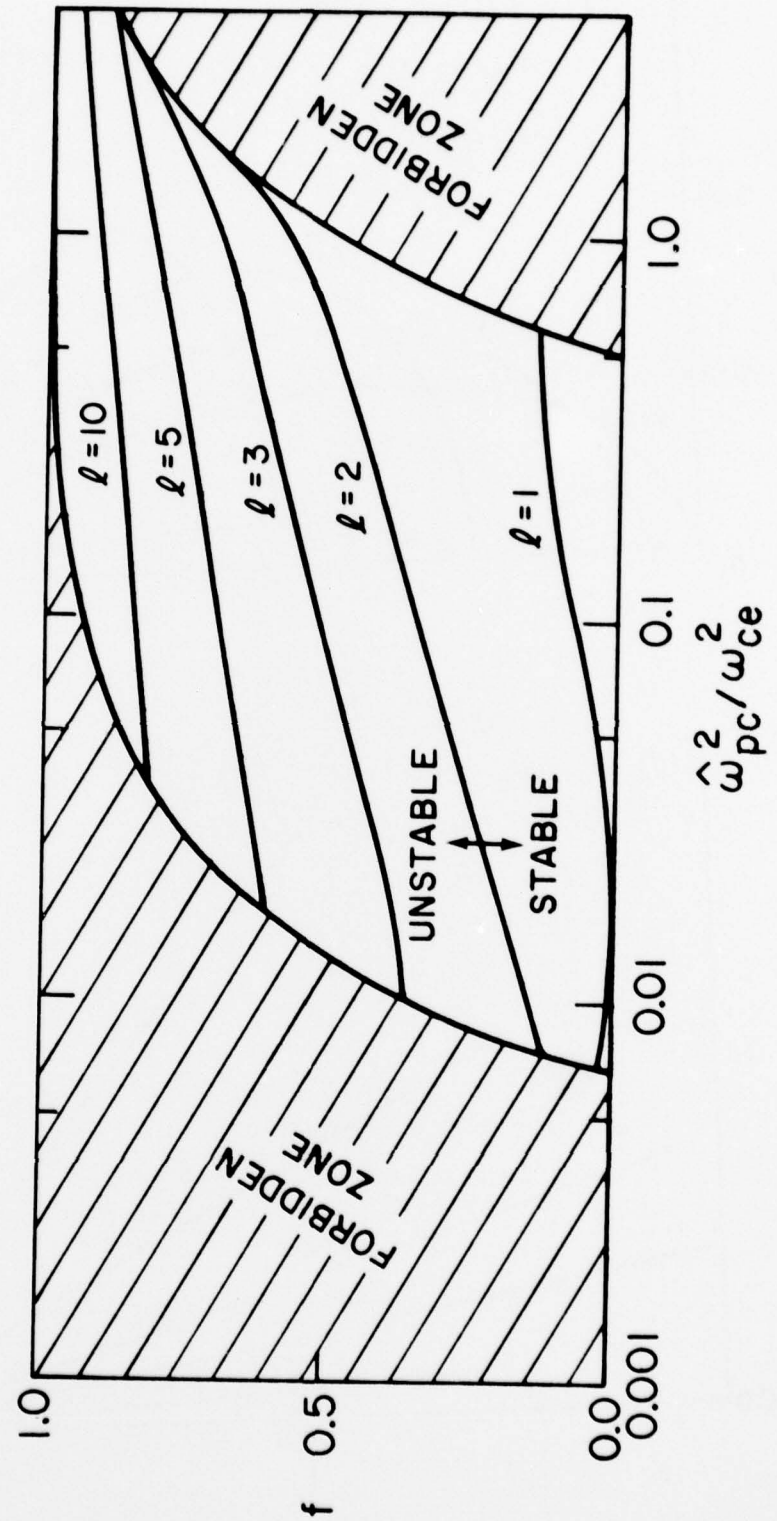
FORBIDDEN ZONE
FORBIDDEN ZONE
UNSTABLE
STABLE
ℓ=10
ℓ=5
ℓ=3
ℓ=2
ℓ=1
1.0
0.1
0.01
0.001
0.0
1.0
0.5
f
$\hat{\omega}_{pc}^2/\omega_{ce}^2$

Fig. 8

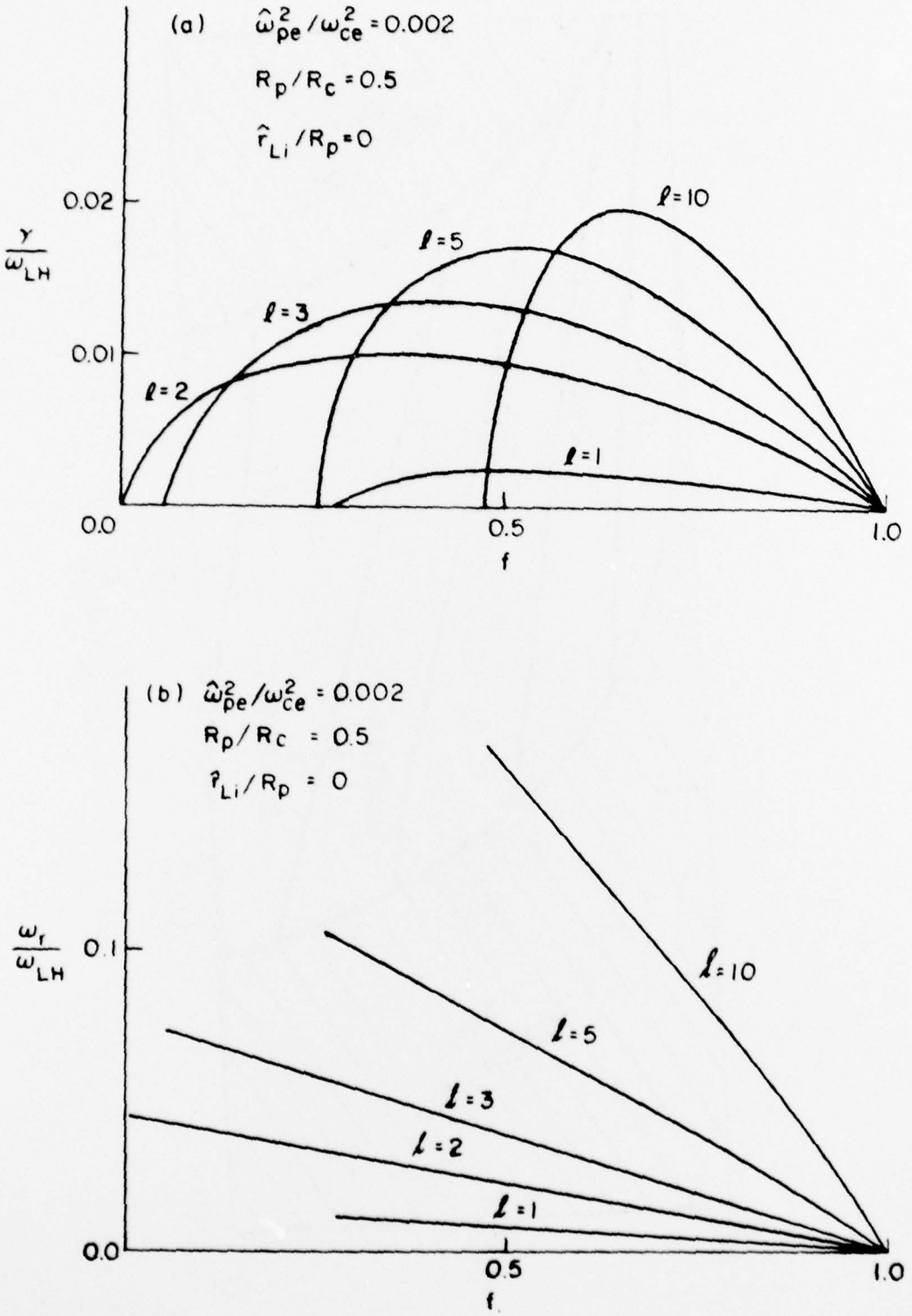
(a) $\hat{\omega}_{pe}^2/\omega_{ce}^2 = 0.002$
$R_p/R_c = 0.5$
$\hat{r}_{Li}/R_p = 0$
$\frac{\gamma}{\omega_{LH}}$
0.02
0.01
0.0
0.5
1.0
f
$\ell = 10$
$\ell = 5$
$\ell = 3$
$\ell = 2$
$\ell = 1$
(b) $\hat{\omega}_{pe}^2/\omega_{ce}^2 = 0.002$
$R_p/R_c = 0.5$
$\hat{r}_{Li}/R_p = 0$
$\frac{\omega_r}{\omega_{LH}}$
0.1
0.0
0.5
1.0
f
$\ell = 10$
$\ell = 5$
$\ell = 3$
$\ell = 2$
$\ell = 1$

Fig. 9

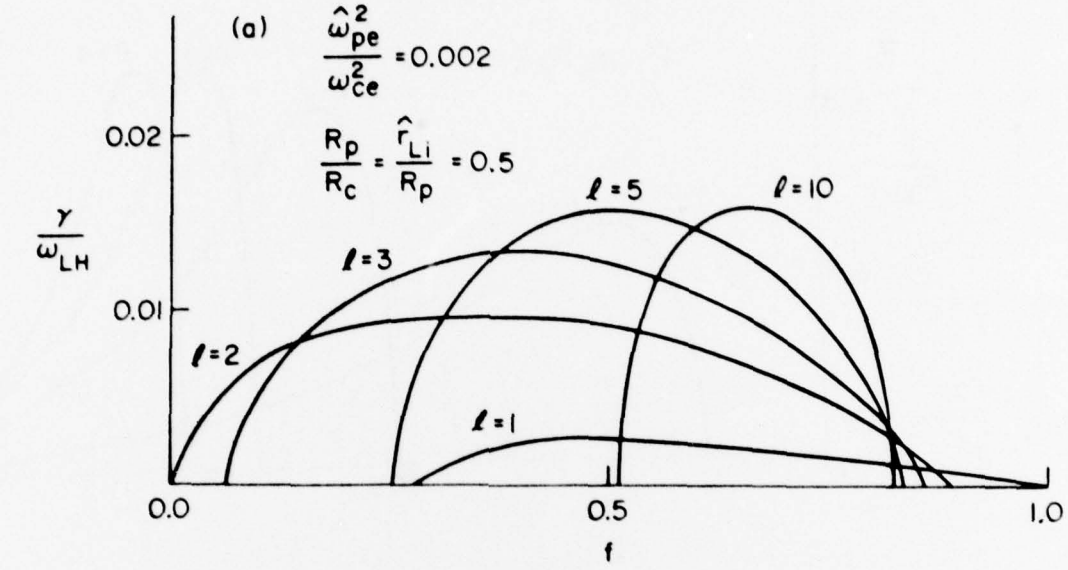
(a)
$\frac{\hat{\omega}_{pe}^2}{\omega_{ce}^2} = 0.002$
$\frac{R_p}{R_c} = \frac{\hat{r}_{Li}}{R_p} = 0.5$
$\frac{\gamma}{\omega_{LH}}$
0.02
0.01
0.0
0.5
1.0
f
ℓ = 1
ℓ = 2
ℓ = 3
ℓ = 5
ℓ = 10

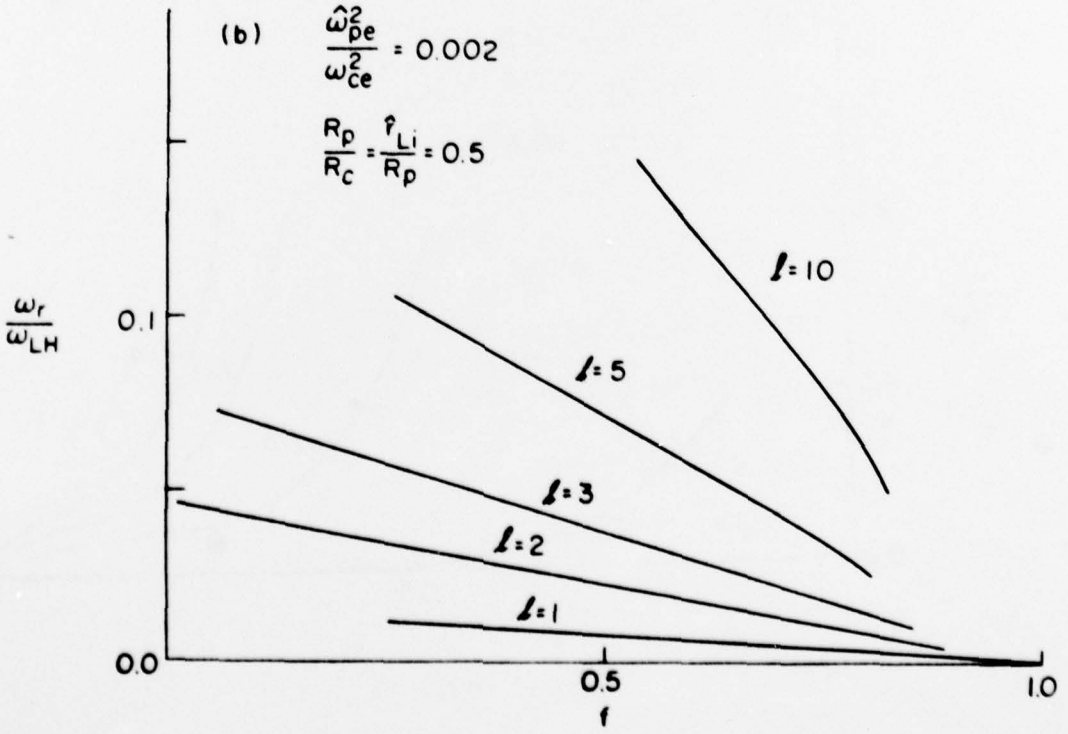
(b)
$\frac{\hat{\omega}_{pe}^2}{\omega_{ce}^2} = 0.002$
$\frac{R_p}{R_c} = \frac{\hat{r}_{Li}}{R_p} = 0.5$
$\frac{\omega_r}{\omega_{LH}}$
0.1
0.0
0.5
1.0
f
ℓ = 1
ℓ = 2
ℓ = 3
ℓ = 5
ℓ = 10

Fig. 10

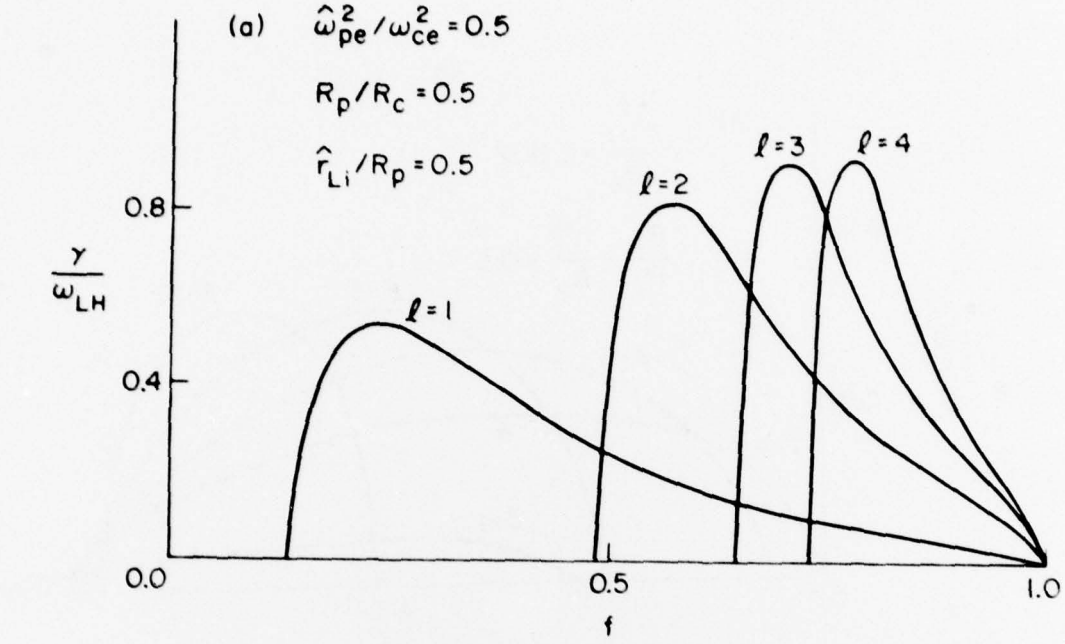
(a)
$\hat{\omega}_{pe}^2/\omega_{ce}^2 = 0.5$
$R_p/R_c = 0.5$
$\hat{r}_{Li}/R_p = 0.5$
$\ell = 1$
$\ell = 2$
$\ell = 3$
$\ell = 4$
$\frac{\gamma}{\omega_{LH}}$
0.8
0.4
0.0
0.5
1.0
f

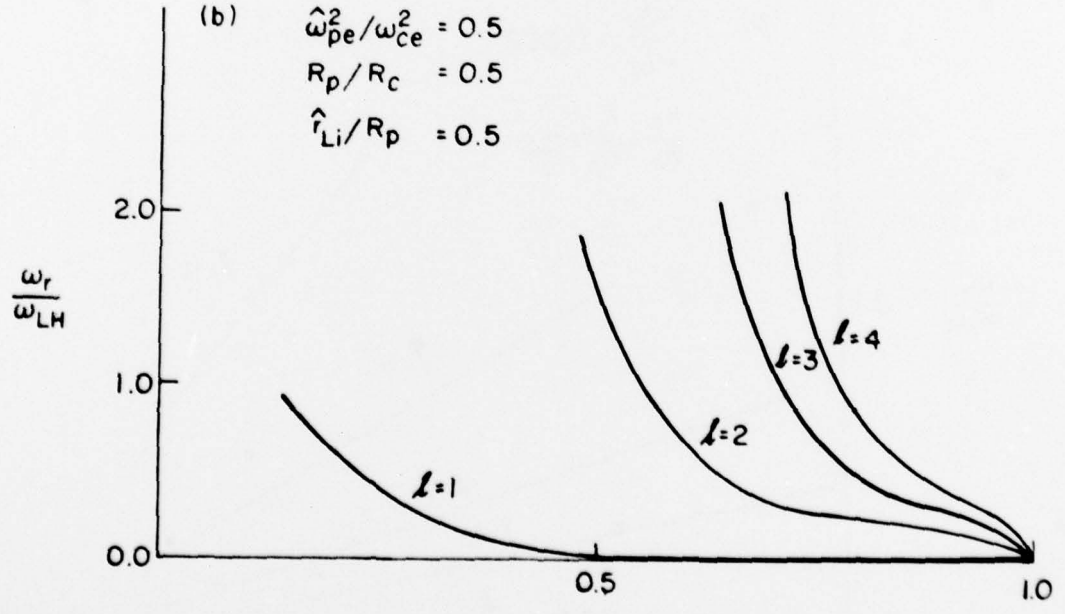
(b)
$\hat{\omega}_{pe}^2/\omega_{ce}^2 = 0.5$
$R_p/R_c = 0.5$
$\hat{r}_{Li}/R_p = 0.5$
$\ell = 1$
$\ell = 2$
$\ell = 3$
$\ell = 4$
$\frac{\omega_r}{\omega_{LH}}$
2.0
1.0
0.0
0.5
1.0

Fig. 11

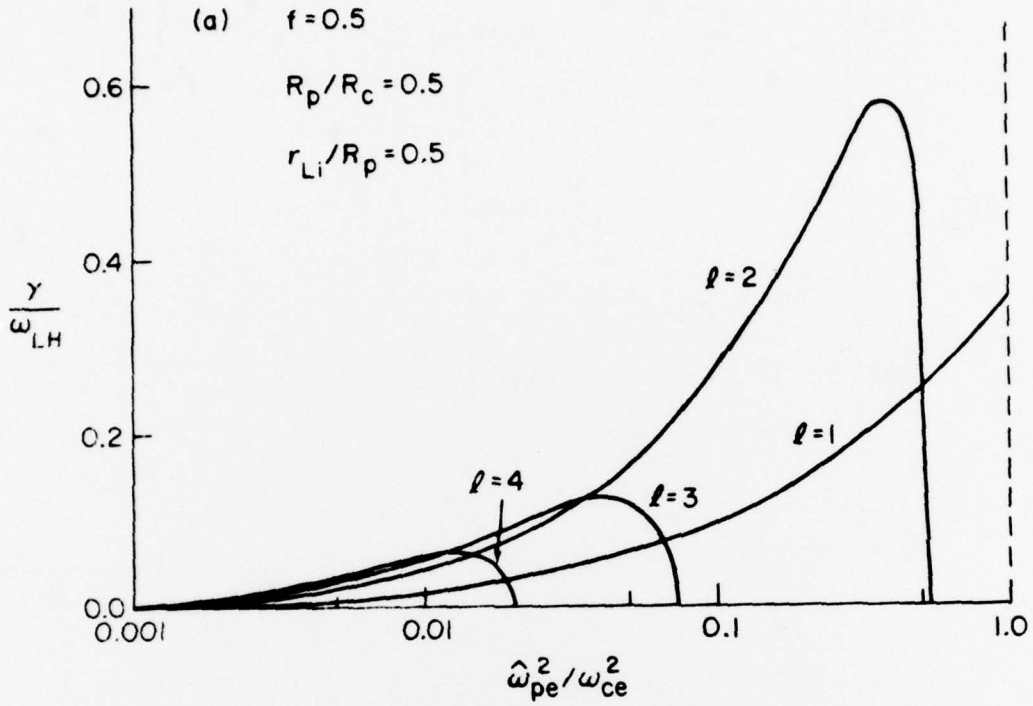
(a)
f = 0.5
$R_p/R_c = 0.5$
$r_{Li}/R_p = 0.5$
$\frac{\gamma}{\omega_{LH}}$
0.6
0.4
0.2
0.0
0.001
0.01
0.1
1.0
$\hat{\omega}_{pe}^2/\omega_{ce}^2$
$\ell = 2$
$\ell = 1$
$\ell = 4$
$\ell = 3$

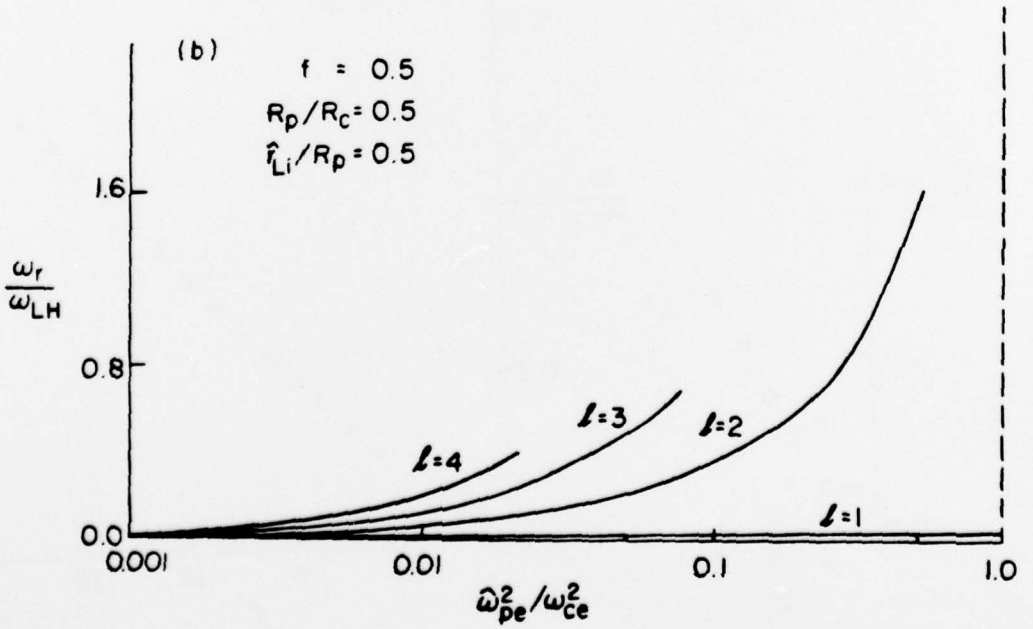
(b)
f = 0.5
$R_p/R_c = 0.5$
$\hat{r}_{Li}/R_p = 0.5$
$\frac{\omega_r}{\omega_{LH}}$
1.6
0.8
0.0
0.001
0.01
0.1
1.0
$\hat{\omega}_{pe}^2/\omega_{ce}^2$
$\ell = 4$
$\ell = 3$
$\ell = 2$
$\ell = 1$

Fig. 12

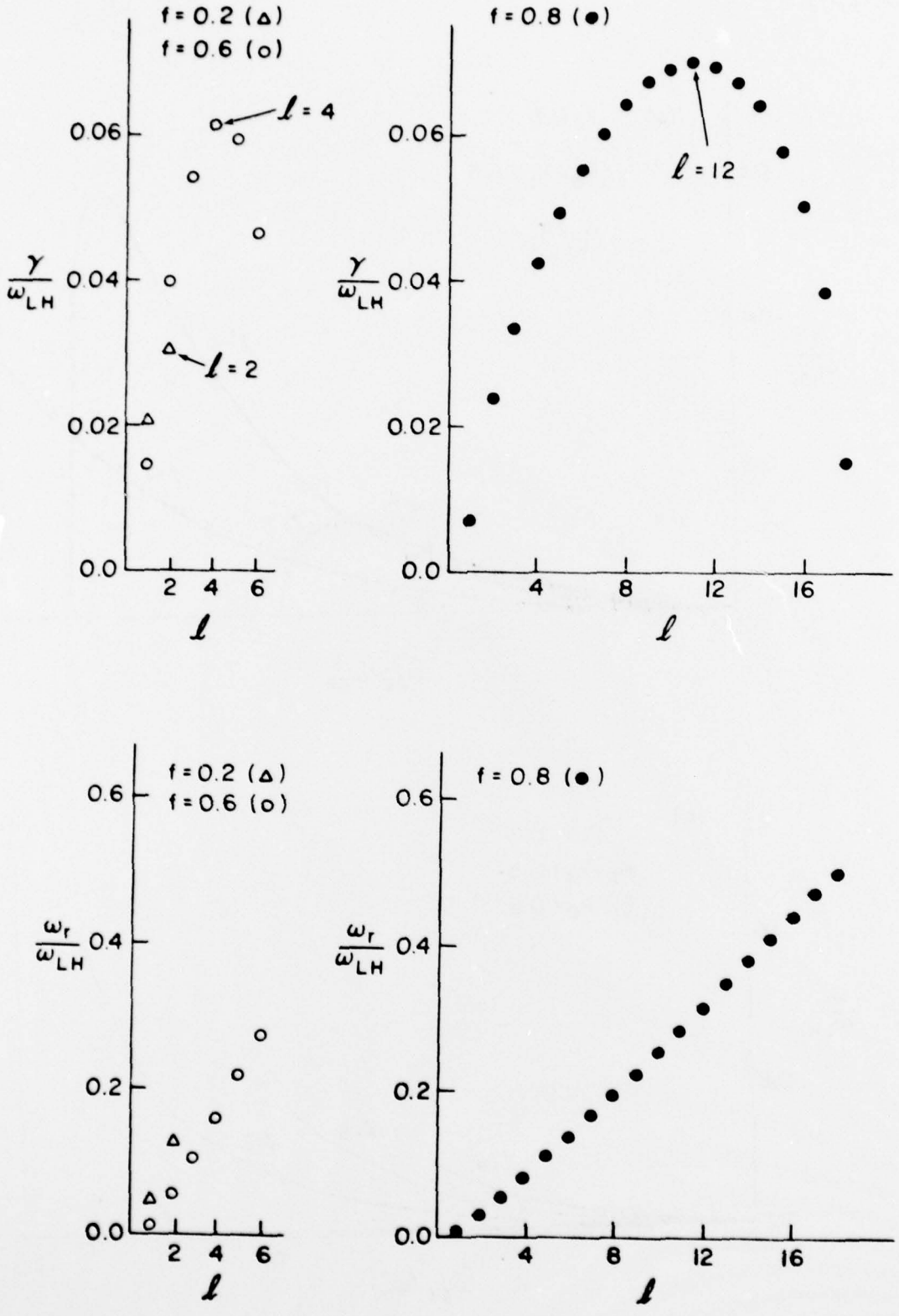
f = 0.2 (Δ)
f = 0.6 (o)
ℓ = 4
ℓ = 2
0.06
0.04
0.02
0.0
γ/ω_LH
2 4 6
ℓ
f = 0.8 (●)
ℓ = 12
0.06
0.04
0.02
0.0
γ/ω_LH
4 8 12 16
ℓ
f = 0.2 (Δ)
f = 0.6 (o)
0.6
0.4
0.2
0.0
ω_r/ω_LH
2 4 6
ℓ
f = 0.8 (●)
0.6
0.4
0.2
0.0
ω_r/ω_LH
4 8 12 16
ℓ

Fig. 13

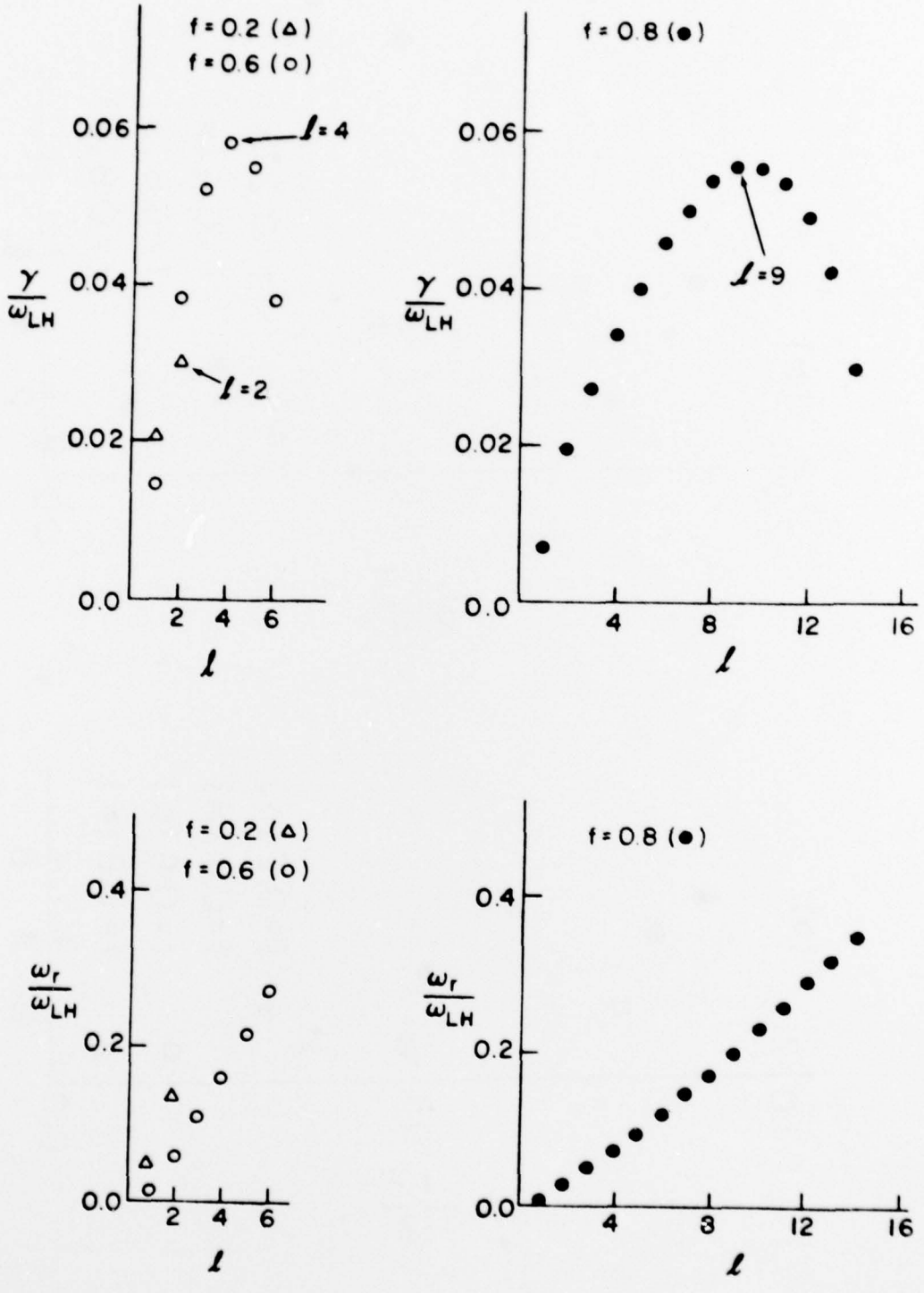
f = 0.2 (Δ)
f = 0.6 (o)
f = 0.8 (●)
γ/ω_LH
ω_r/ω_LH
l = 4
l = 2
l = 9
l
0.0
0.02
0.04
0.06
0.2
0.4
2
4
6
8
12
16

Fig. 14

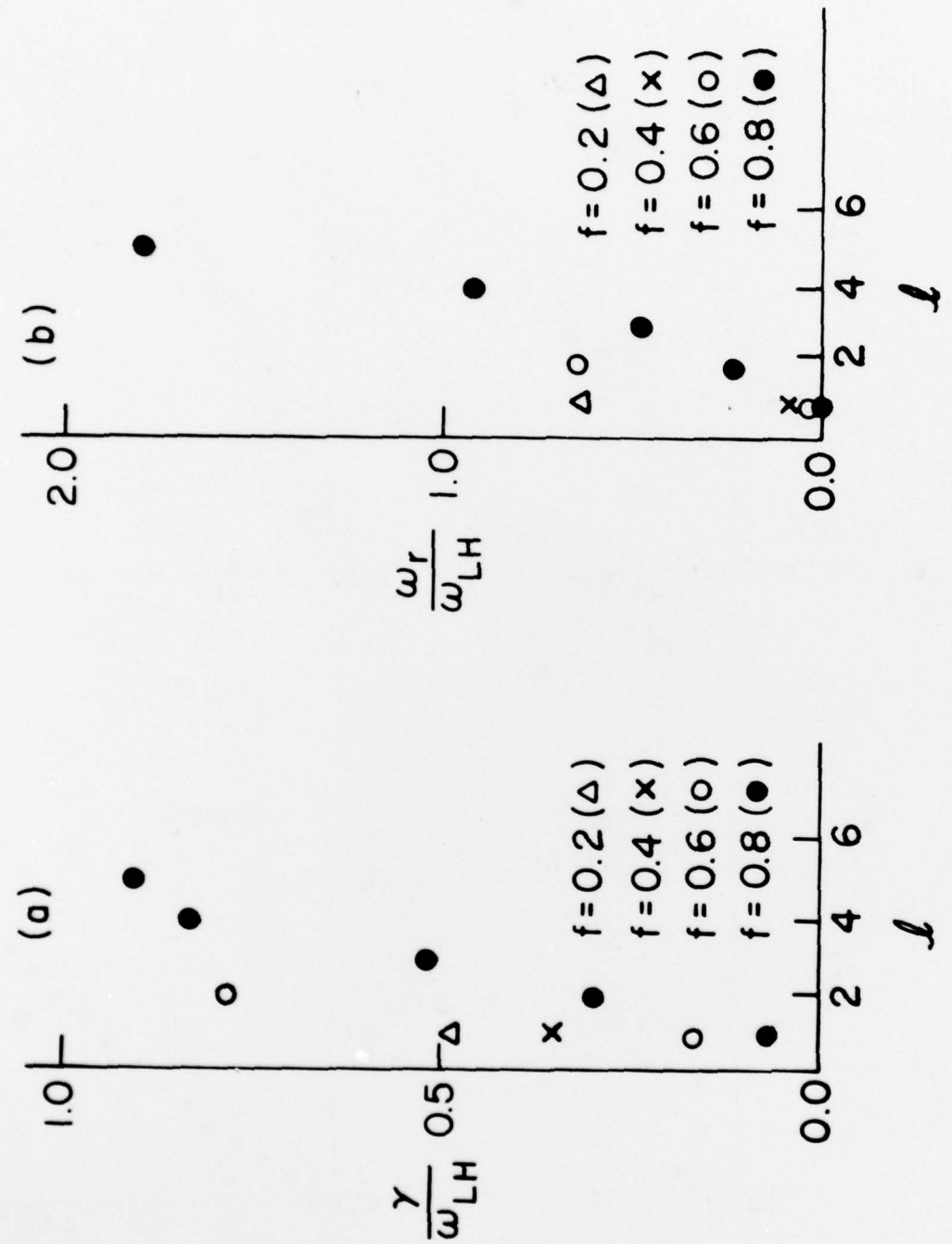
(a)
(b)
1.0
0.5
0.0
2.0
1.0
0.0
$\frac{\gamma}{\omega_{LH}}$
$\frac{\omega_r}{\omega_{LH}}$
2
4
6
l
f=0.2 (Δ)
f=0.4 (x)
f=0.6 (o)
f=0.8 (●)

Fig. 15